AD-A233 293 `FILE COPY`

⑪

`RTI`

RESEARCH TRIANGLE INSTITUTE

SEMICONDUCTOR DIAMOND TECHNOLOGY

DTIC
ELECTE
MAR 15 1991
S D
D

R. J. Markunas
R. A. Rudder
J. B. Posthill
R. E. Thomas

STRATEGIC DEFENSE INITIATIVE ORGANIZATION
Innovative Science and Technology Office

REPORT DOCUMENTATION PAGE

Public reporting burden for this collection of information is estimated to average 1 hour per response, including the time for reviewing instructions, searching existing data sources, gathering and maintaining the data needed, and completing and reviewing the collection of information. Send comments regarding this burden estimate or any other aspect of this collection of information, including suggestions for reducing this burden to Washington Headquarters Services, Directorate for Information Operations and Reports, 1215 Jefferson Davis Highway, Suite 1204 Arlington, VA 22202-4302, and to the Office of Management and Budget Paperwork Reduction Project (0704-0'88), Washington, DC 20503

1. AGENCY USE ONLY *(Leave blank)*	2. REPORT DATE	3. REPORT TYPE AND DATES COVERED
		Final Report, 1 January, 1990 – 31 December, 199

4. TITLE AND SUBTITLE	5. FUNDING NUMBERS
Semiconductor Diamond Technology	
6. AUTHOR(S) R.J. Markunas, R.A. Rudder, J.B. Posthill, R.E. Thomas	N00014-86-C-0460

7. PERFORMING ORGANIZATION NAME(S) AND ADDRESS(ES)	8. PERFORMING ORGANIZATION REPORT NUMBER
Research Triangle Institute P.O. Box 12194 Research Triangle Park, NC 27709	83U-3629

9. SPONSORING/MONITORING AGENCY NAME(S) AND ADDRESS(ES)	10. SPONSORING/MONITORING AGENCY REPORT NUMBER
Office of Naval Research 800 N. Quincy Street Arlington, VA 22217-5000	

11. SUPPLEMENTARY NOTES

12a.DISTRIBUTION/AVAILABILITY STATEMENT	12b.DISTRIBUTION CODE
Approved for public release; unlimited distribution	

13. ABSTRACT *(Maximum 200 words)*

This report summarizes results from the 1990 Semiconducting Diamond Technology Program at Research Triangle Institute. The advancement of existing technologies such as the low pressure rf-plasma assisted CVD technology has allowed the development of new techniques for diamond deposition. The research has emphasized growth techniques for enhancing diamond heteronucleation Highlights for this year are listed below:

- Epitaxial lateral overgrowth was demonstrated;
- Diamond Schottky devices were fabricated with Li doping;
- Boron doped IGFETs were fabricated and tested;
- Gas analysis identified C_2H_2 by-product;
- Mo interlayers were deposited on Ni for heteronucleation studies;
- Hydrogen-halogen exchange reactions were demonstrated;
- A CF_4/H_2 system produced direct nucleation on Si(100);
- Nucleation enhancement local to graphite fibers was demonstrated.

14. SUBJECT TERMS	15. NUMBER OF PAGES
	63
	16. PRICE CODE

17. SECURITY CLASSIFICATION OF REPORT	18. SECURITY CLASSIFICATION OF THIS PAGE	19. SECURITY CLASSIFICATION OF ABSTRACT	20. LIMITATION OF ABSTRACT
UNCLASSIFIED	UNCLASSIFIED	UNCLASSIFIED	

TABLE OF CONTENTS

Accesion For

NTIS CRA&I	
DTIC TAB	
U.	
J.	

By
D..t ib ...

Av. ...

D..t

A-1

i

1.0 INTRODUCTION

This is the final report for 1990 on the Semiconducting Diamond Technology program at Research Triangle Institute. The report highlights accomplishments in several areas critical to the development of semiconducting diamond. Those areas are:

- low pressure rf-plasma assisted chemical vapor deposition.

- development of atomic layer epitaxy technology,
  thermal F_2/CH_4 work
  surface chemistry studies

- metal substrate development for heteronucleation.

In addition to the progress in those areas, the report also includes a copy of an article submitted for publication in Appl. Phys. Lett. entitled *Direct deposition of polycrystalline diamond on Si(100) substrates without substrate pretreatment.* This letter describes an exciting new technique for diamond deposition using 8% CF_4 in H_2 discharges. The low pressure rf discharges have been able to nucleate diamond on as-received silicon substrates without any pretreatment of the surfaces such as diamond scratching or oiling. The technique is a promising technique for thin film diamond applications and in areas where increased nucleation would lead to increased adhesion and smoother topographies.

Besides the CF_4/H_2 technique. diamond heteronucleation has been promoted by locating graphite fibers in the immediate vicinity of candidate substrates for diamond growth. Substrates such as silicon, fused silica, crystalline quartz, and nickel have all shown increased diamond nucleation from the presence of the fibers. These substrates, like the substrates used in the CF_4/H_2 work, were not diamond scratched prior to

1

exposure in this case to 2% CH$_4$ in H$_2$ discharges. The exact role of the graphite fibers in promoting heteronucleation has not been resolved at this time. It is speculated that gasification products from the the graphite fibers are promoting diamond nucleation. These products, if circulated into the high temperature plasma region, would be converted into the stable-high-temperature products. By locating the fibers near the substrate surface, these products are not converted before they arrive at the substrate surface. An abstract has been submitted to the Applied Diamond Conference in Auburn 1991. This abstract is included in this report.

2.0   PROGRESS IN LOW PRESSURE rf-PLASMA ASSISTED CVD

Previous work in 1989 at Research Triangle Institute had demonstrated both polycrystalline and homoepitaxial growth of diamond at pressures between 0.50 and 10.0 Torr using a low pressure rf-plasma assisted CVD system. Both the polycrystalline and homoepitaxial diamond films exhibited sharp 1332 cm^{-1} Raman signatures with the polycrystalline material also containing varying degrees of non-diamond bonding. Some homoepitaxial films and almost all polycrystalline films exhibited a broad photoluminescence background. Homoepitaxial films deposited by the low pressure rf-plasma assisted technique at temperatures ≥ 650 °C showed no photoluminescence. These films were indistinguishable in the Raman from the substrate itself. Secondary electron microscopy (SEM) of the homoepitaxial layers show the topography to be extremely planar. Scratch lines remaining from the mechanical polish of the substrate are not apparent on the substrate after film growth.

This year, we continued development of the low pressure rf-plasma assisted CVD technique. More fundamental characterizations of the plasma were made. Epitaxial lateral overgrowth of silicon patterned diamond substrates were achieved. Doping of homoepitaxial layers with lithium and boron was accomplished. Functional test devices were fabricated which began to give insights into modifications of the fabrication process for improved device performance. In conjunction with Kobe Research and Development Corporation, Schottky diode devices were fabricated and tested using Li doped homoepitaxial layers.

2.1 Gas Phase Analysis of Low-Pressure rf-Discharges

Emission and mass spectroscopy have been used to better characterize the growth conditions for diamond deposition using the CH_4 in H_2 discharges. The low-pressure high-power plasma is seen to be a chemically reactive plasma creating atomic hydrogen. converting CH_4 into C_2H_2, and gasifying graphite or other solid carbon sources into C_2H_2. As discussed in the 1990 quarterly reports, the discharges can be classified in a low power and a high power state. At low rf power levels. the discharge of 1% CH_4 in H_2 is bluish in color and had been designated "blue" mode. In the blue mode. emission from CH Swann bands and the antibonding state of molecular H_2 are observed. Transitions from the antibonding state of molecular H_2 to a bonding state occur over a wide frequency range and hence produce a continuim of emission. Statistically. about 5% of antibonding molecular H_2 dissociated into atomic hydrogen. Considering that probably only a small percentage of the neutral H_2 is excited, the "blue" mode is not an efficient generator of atomic hydrogen.

At higher rf power levels, the impedance of the hydrogen discharge reduces allowing more power coupling to the gas. The discharge becomes instantly red in color. The high power mode of operation has been designated "red" mode in previous quarterly reports. In the red mode. emission from the H_α, H_β, and H_δ, ($n = 3 \rightarrow 2$. $n = 4 \rightarrow 2$, and $n = 5 \rightarrow 2$) states are clearly evident. It is important to note that observed transitions are from atomic hydrogen states. and are direct evidence of atomic hydrogen in the plasma. The effective electron temperature of the atomic hydrogen population has been calculated assuming a Boltzman distribution to the population and

4

comparing relative intensities of the H_α and the H_β transitions in the Balmer series. Table I shows that the effective temperature of the discharge remained approximately the same for the pressure series from 1 to 10 Torr. This occurred despite the factor of 6 reduction in rf power input.

Table 1

Pressure	Flow rate (sccm)	Estimated rf power (w)	T_{plasma} (K)
10	12.5	1200	3270
7	8.8	900	3200
5	6.3	500	3200
3	3.8	330	3350
1	1.3	200	3420

Besides emission spectroscopy, mass spectroscopy has been used to establish the effluents of chemical species from the discharge. At pressures from 10 to 1 Torr under the same flow rate and power conditions as reported in Table 1, a conversion of CH_4 to C_2H_2 of about 40% is observed with some percentage of the hydrocarbons being depleted from the gas. These experiments were conducted without the graphite stage in the reactor. With the graphite stage 3.0 mm below the discharge, C_2H_2 production was observed at levels greater than the original CH_4 counts. Gasification of the graphite stage is a major source of C_2H_2 in the low pressure rf discharges. Figure 2.1 shows the pressure dependence observed from 1 - 10 Torr for the production of C_2H_2. This observation of C_2H_2 as the dominant gasification product as opposed to CH_4 is

supported by modulated atomic hydrogen beam experiments performed by M. Balooch and D.R. Olander, J. Chem. Phys **63**, 4772 (1975). Figure 2.2 in this report is a duplication of Figure 5 from the J. Chem. Phys. paper. The figure shows that there are two temperature regions upon which there is gasification of the graphite. Below 800 K, CH_4 is the sole gasification product. Above 1000 K , C_2H_2 is produced. Between 800 and 1000 K, the atomic hydrogen is recombined on the graphite with no gasification occurring.

2.2   Epitaxial Lateral Overgrowth

Epitaxial diamond overgrowth on Si patterns on natural diamond substates has been demonstrated using low pressure rf plasma-assisted chemical vapor deposition. The plasma-assisted technique uses a 13.56 MHz rf generator and inductive coupling to excite gas mixtures of H_2, CH_4 and CO at a reduced pressure of 5 Torr. The overgrowth was approximately isotropic, extending laterally over the Si pattern by 0.45 μm while vertical growth was 0.50 μm.

The thermal and electrical properties of diamond make it an excellent candidate for high speed, high power transistors. A number of significant problems must be overcome before the potential of diamond can be realized. These problems include the unavailability of n-type dopants and the lack of a suitable substrate for heteroepitaxy. However, a number of useful devices can be fabricated with epitaxial p-type layers. Grot et al. have reported the fabrication of an insulated gate field effect transistor (a depletion mode device). Others have reported Schottky diodes and Schottky-gate

field effect transistors. The development of any material to its full electronic potential depends critically on the support technologies such as metallization, etching, epitaxy, passivation, etc. In silicon microelectronics, selected-area growth is now allowing the fabrication of sophisticated three-dimensional devices. In GaAs, selected-area growth is found to pin substrate defects to the area of epitaxial growth above the original seed window. Few defects are observed to propagate into the epitaxial overgrowth.

We reported, in Crystal City, on successful diamond epitaxial overgrowth of Si patterns that were lithographically defined on natural diamond (100) substrates. Given the difficulty of diamond nucleation on non-diamond materials, the selectivity for homoepitaxial growth on the exposed diamond seems assured. The challenge is then to have a mask material that 1) does not dissolve rapidly under the atomic hydrogen ambient, and 2) does not spontaneously nucleate diamond growth which would not be in registry with the advancing diamond growth front that is propagating across the mask. A polycrystalline Si mask was used for this study. Previous work in the low-pressure rf-plasma assisted chemical vapor deposition system had always used scratched Si substrates for polycrystalline diamond growth. Deposition on Si wafers which had not been diamond scratched produced only a few scattered particles of diamond. The nucleation density, thus, is very low in this deposition system for unscratched Si. While Si does dissolve under an atomic hydrogen environment, the reaction rate decreases with increasing temperature. A slow dissolving of the mask material might be beneficial, allowing early stages of carbon nucleation on the Si surfaces to be undercut by an atomic hydrogen etch. In our study, we observed that a

400 Å thick Si mask did dissolve producing small areas of homoepitaxial growth. Consequently, a 2000 Å thick Si mask was employed. The thicker mask did not dissolve during the growth. Some spontaneous diamond nucleation was observed, but the density of nucleation was low.

The diamond substrates were subjected to a standard RCA clean followed by polycrystalline Si deposition in a MBE growth system (Si deposition performed by T.P. Humphreys, NCSU). Standard lithography was used to open holes in the Si layer where homoepitaxial growth could nucleate. Following diamond deposition. the samples were characterized using scanning electron microscopy (SEM) and micro-Raman spectroscopy. SEM showed smooth epitaxial growth above the window areas. This growth extended beyond the lithographically defined area. Figure 2.3 shows plan-view SEM micrographs of the pattern used for the overgrowth experiments. The bright regions are regions of diamond growth. The dark regions are regions of Si. In the higher magnification, one sees that (1) the window areas are extremely smooth. (2) some spontaneous nucleation has occurred on the Si mask, and (3) the overgrowth areas show a roughened edge due to crystal facetting. Crystal facetting on overgrowth is a common occurrence in Si overgrowth of SiO_2 islands.

Micro-Raman has also been used to examine the epitaxial overgrowth. A micro-Raman spectrum taken from the region above the diamond window. The spectrum shows a 1332 cm^{-1} diamond line with a full-width-half-maximum (FWHM) of 3.4 cm^{-1}. The FWHM measured here is at the resolution limit of the instrument. The beam focus is approximately 1 μm in spot size. A micro-Raman spectrum taken with the

beam centered on a region of overgrowth. This spectrum shows a 1332 cm^{-1} line with a FWHM of 3.5 cm^{-1}, very close to the 3.4 cm^{-1} taken from the homoepitaxial growth above the window. In contrast, a micro-Raman spectrum was taken from one of the diamond crystallites which spontaneously nucleated on the Si. It shows a 1332 cm^{-1} line with a broadened FWHM of 5 cm^{-1}. The FWHM of 5 cm^{-1} is what is typically seen on polycrystalline films. This contrast in FWHM illustrates the importance of the "seed" in the quality of the film growth. Under identical plasma and growth conditions, growth from a diamond seed produces better diamond than growth from a site on the Si that had spontaneously nucleated.

Finally, the overgrowth was illucidated by chemically etching the Si from the diamond. Figure 2.4 shows SEM of a cleaved cross-section showing diamond epitaxial lateral overgrowth. The sample has been sputter-coated with $\sim$ 100 Å of Pt to prevent charging. The left photograph shows the smooth epitaxial growth and facetting on the overgrowth. Notice the scratches (remnants from polishing) that are on the diamond surface that had been covered by Si during the overgrowth experiments. The right photograph in Figure 2.4 gives a measure of the lateral overgrowth. The overgrowth appears to be isotropically advancing by 0.45 μm laterally and 0.50 μm vertically.

Epitaxial lateral overgrowth has been demonstrated using a low pressure rf-plasma assisted chemical vapor deposition technique. A 2000 Å thick Si mask has been used to define the diamond "seeds". The Si shows some spontaneous nucleation, but the density of nucleation is low. The overgrowth is isotropic, extending over the Si mask

0.45 μm and above the mask 0.50 μm. Some facetting is observed on the overgrowth areas. Micro-Raman analysis shows the overgrowth areas to have a FWHM comparable to the homoepitaxial layers deposited above the diamond windows. This was contrasted by a FWHM of 5 cm^{-1} from a polycrystalline diamond that nucleated spontaneously on the Si mask.

2.3 Fabrication and Testing of a Diamond IGFET

A transistor structure was fabricated using the extremely selective nature of the diamond deposition process to deposit diamond only on areas where holes were exposed through a silicon mask. The transistor structure was fabricated on a Type 1A natural diamond (100) substrate from Drucker. The diamond substrate was cleaned using a conventional RCA wet chemical clean. A 700 Å film of polycrystalline silicon was deposited on the substrate. The silicon was patterned using standard lithographic techniques and wet etching to open holes for deposition of the conducting p-type diamond areas. Following diamond deposition, the silicon mask was etch removed. The sample was then coated with a 250 Å remote plasma enhanced CVD (RPECVD) SiO$_2$ gate dielectric. Titanium gate electrodes were formed using liftoff. Source-drain contact openings were patterned and openings etched in the oxide using buffer HF solution. Titanium contacts were formed using liftoff. The contacts were relatively ohmic as deposited. The gate length and width of the transistors was 8 μm and 50 μm, respectively. A schematic of the device structure is shown in Figure 2.5.

The IGFET source drain IV characteristics are shown in Figure 2.6. The device showed transistor action characteristic of a p channel, depletion mode device. There is some indication of saturation in the 6 to 8 V region. The device cannot be pinched off with the available gate voltage. The leakage current is most likely due to defects in the homoepitaxial material or surface leakage. The maximum transconductance of the device is 38 μS/mm at 8 V drain to source. The transconductance of the device is slightly larger for the 1 to 2 V gate step than for the 0 to 1 V gate step. This increase in transconductance with increasing depletion is indicative of a relatively high density of surface states at or near the diamond/SiO$_2$ interface. The geometry of the FET is such that the source to gate resistance is on the order of 2×10^5 Ω. This resistance would decrease the transconductance of the device by a factor of about 2.

Characterization of the IGFET device described in this paper indicates that the diamond/SiO$_2$ interface has a high interface state density leading to degraded device performance. The RPECVD SiO$_2$ process is currently used to fabricate high performance Si MISFETs (G$_{max}$ $\sim$ 75 mS/mm at a gate length of 2 μm with μ_{eff} = 800 cm^2/V-s), thus more effective surface treatments of the diamond surface either during the termination of the growth or prior to SiO$_2$ deposition are needed to achieve high performance IGFETs. Recently, we have chemically etched the gate and electrode materials from the diamond IGFET. SEM micrographs of the diamond source-drain-channel areas show high contrast near the periphery of those areas. It is suspected that the silicon mask used to selectively define the doped diamond deposition may have allowed some deposition or reaction to occur under the mask area

11

whereby a conductive non-diamond surface layer could have formed. Elimination of this effect will be critical for improved device performance.

2.4   Investigation of In Situ Li Doping of CVD Diamond

One of the current deficiencies in diamond-based electronics is the lack of suitable n-type dopant. Although there have been specific reports of the formation of n-type diamond, this is still an area that requires further development. Li has been proposed as a potential n-type dopant for diamond based on theoretical modelling. We have undertaken a preliminary study to investigate the suitability of using LiF as a solid source to dope diamond growing in a plasma-enhanced chemical vapor deposition (PECVD) environment.

Type Ia and IIa natural (100) diamond crystals were used in these studies. Lithium doping was accomplished via introduction of a solid source of LiF on the graphite susceptor during the deposition, or via introduction of the solid source to "dose" the reactor prior to loading the substrate for diamond growth. It was found that under diamond growth conditions. the LiF is dissolved by the atomic hydrogen in the reactor. Lithium emissions were observed in the reactor once the sources began to volatilize.

Homoepitaxial films doped with Li were found to be p-type by Hall measurements. For one film, the carrier concentration at room temperature was $\sim 2.8 \times 10^{16} \text{cm}^{-3}$, p-type, with a mobility of $\sim 143 \text{ cm}^2/\text{V-sec}$. Variable temperature conductivity shows

the activation energy, E_a, to be 0.23 eV. We have consistently observed p-type conductivity in diamond homoepitaxial films when Li is introduced in the manner described above. Figure 2.7 shows an I-V trace taken from a Schottky contact (formed by Au evaporation on the surface). This provides further verification of p-type conductivity. There is good rectification, with a breakdown of $\sim$ 6V and a reverse leakage current of $<$ 1 nA. The electron-beam induced current (EBIC) mode of the scanning electron microscope (SEM) was used to estimate the minority-carrier diffusion length. The Schottky contact was used for charge collection, and the induced current was measured as a function of distance, in plan-view, from the contact. Figure 2.8 shows the EBIC trace as function of distance from the Au contact.

For primary beam energies from 10 keV - 20 keV, the minority-carrier diffusion length was measured to be, L_{eff} = 0.5 μm. This compares with EBIC-measured minority-carrier diffusion lengths of $\sim$ 3 μm in natural type IIb diamond (B-doped). Micro-Raman spectroscopy was employed to assess the crystalline quality of homoepitaxial diamond films. The micro-Raman spectrum shows the 1332 cm^{-1} diamond LO phonon line with a FWHM of 3.0 cm^{-1}. This spectrum was obtained by focusing the incident laser beam (Ar$^+$, 514.5 nm) of $\sim$ 5 μm spot size onto the surface of the diamond homoepitaxial film. The 3.0 cm^{-1} Raman line indicates high quality diamond growth. Examining the back side of the diamond substrate also showed a FWHM of 3.0 cm^{-1}.

We currently have no evidence that unintentionally incorporated boron is responsible for the observed p-type conductivity. Films grown without adding a dopant

source are so highly resistive that the type cannot be ascertained. Furthermore, the work report herein was done before any intentional introduction of boron into the reactor. We have also observed differences in the mobility and carrier concentration from film to film. Variations in Li concentration due to use of a solid-source for Li doping and/or the variable quality of the diamond substrates are likely reasons for this. It is suggested that future research in this area utilize a liquid or gas phase source for more controlled introduction of Li into the growth environment. We have currently obtained a source of n-butyl lithium in hexane for addition to the gas stream as an in situ dopant.

FIGURE 2.1.

15
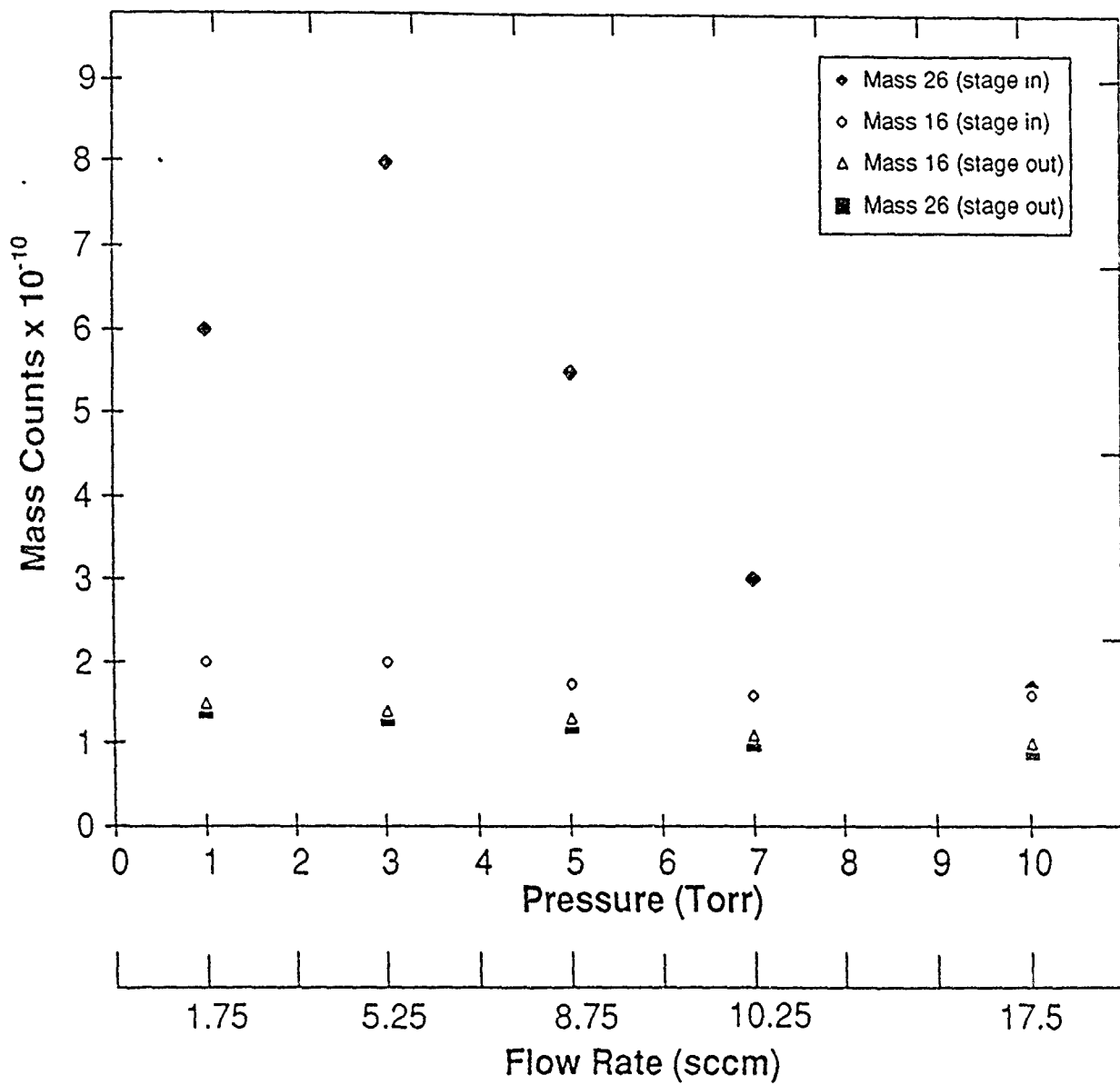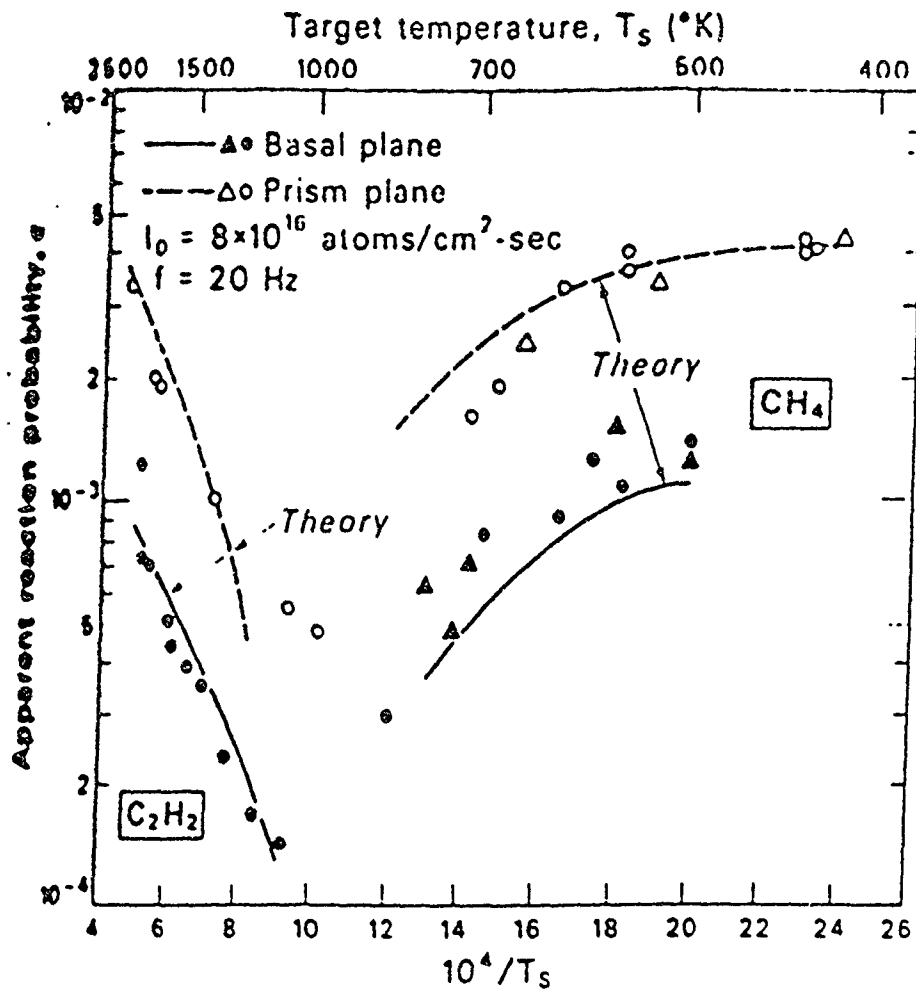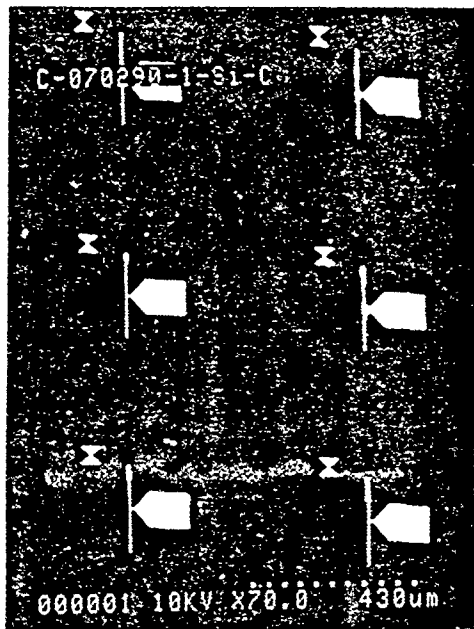
FIGURE 2.2.

Pattern Used
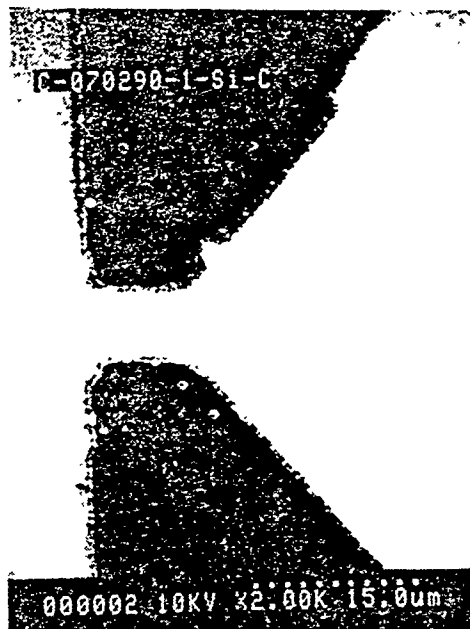
Higher Magnification
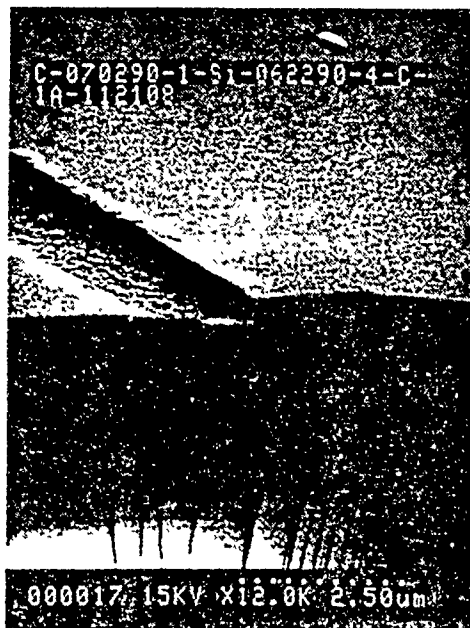
Cleaved Cross-Section

**FIGURE 2.3.**
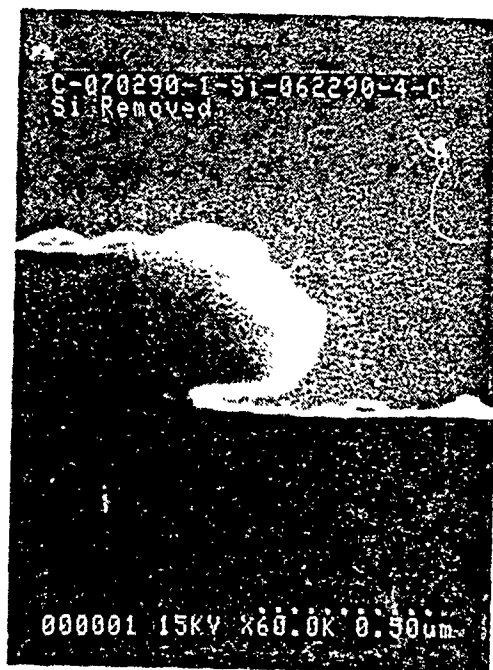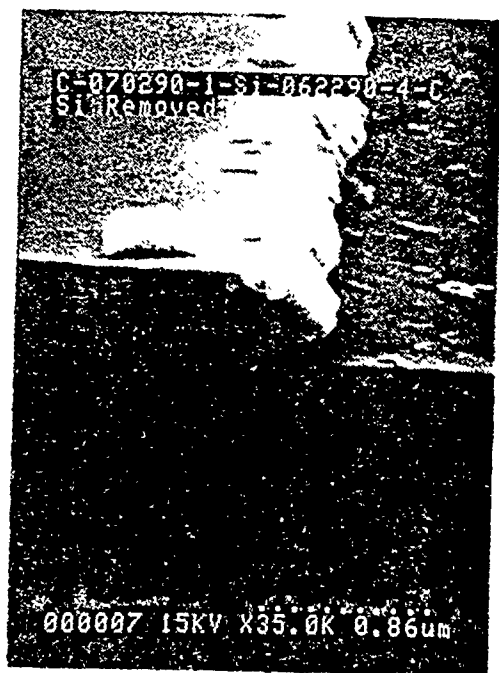
FIGURE 2.4.

Diamond FET by Selective Epitaxy

Silicon or
SiO2 mask →

Diamond →
Substrate

Selective p type
Diamond Epi

Deposited   Gate
Oxide   Contact

Ohmic Source/
Drain contacts
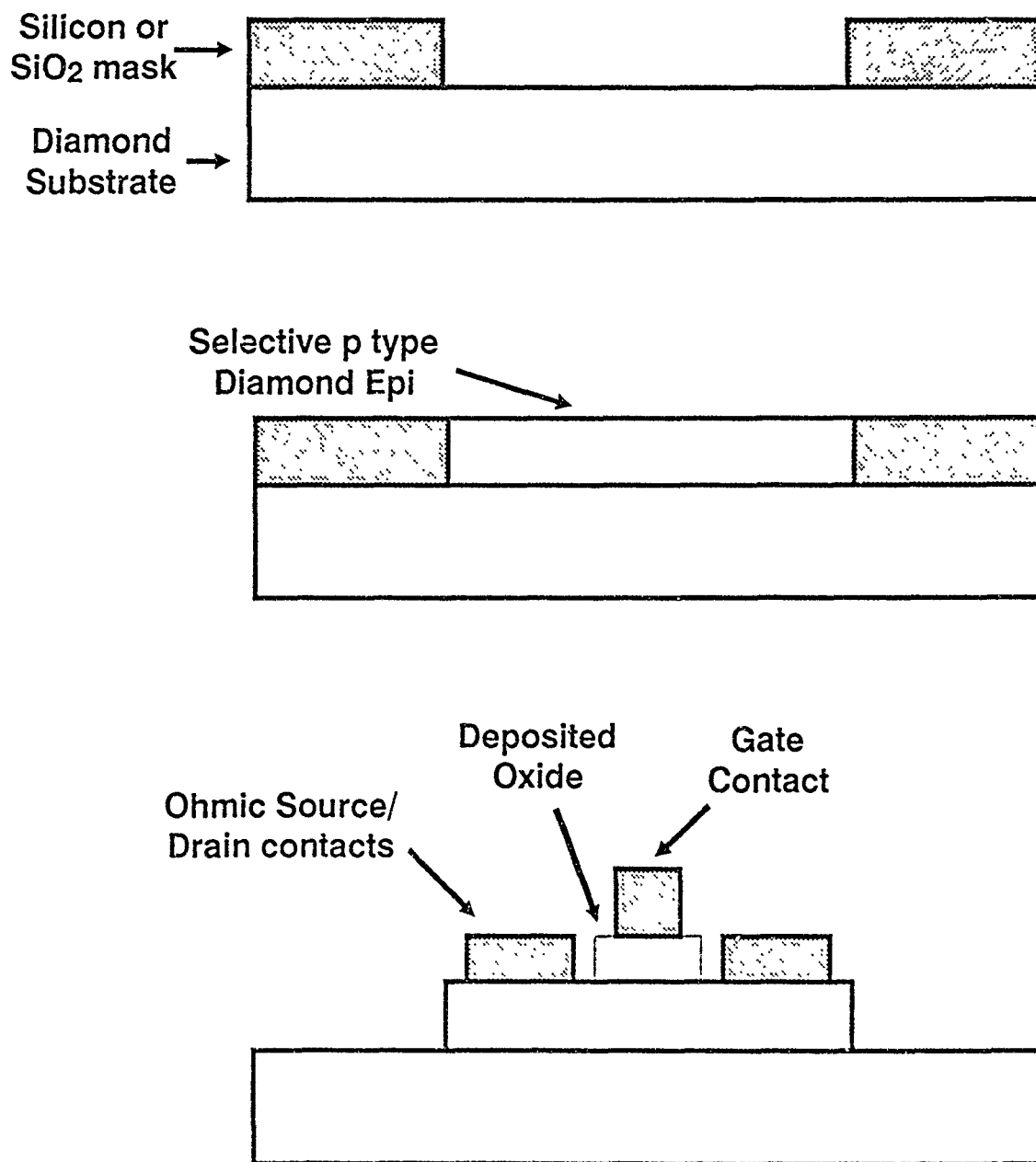
FIGURE 2.5.

SAMPLE ID   : DIAMOND FET
TEST DATE   : 09/13/90
FILE NAME   : d_fet1.o2   RAMP RATE   : 1.0 V/S
GATE WIDTH   : 5.00E-2 mm   # GATE STEPS : 3.00
GATE LENGTH : 8.00E-3 mm   GATE START   : 0 Volts
GM (MAX)   : .0377 mS/mm   GATE STEP   : 1 Volts
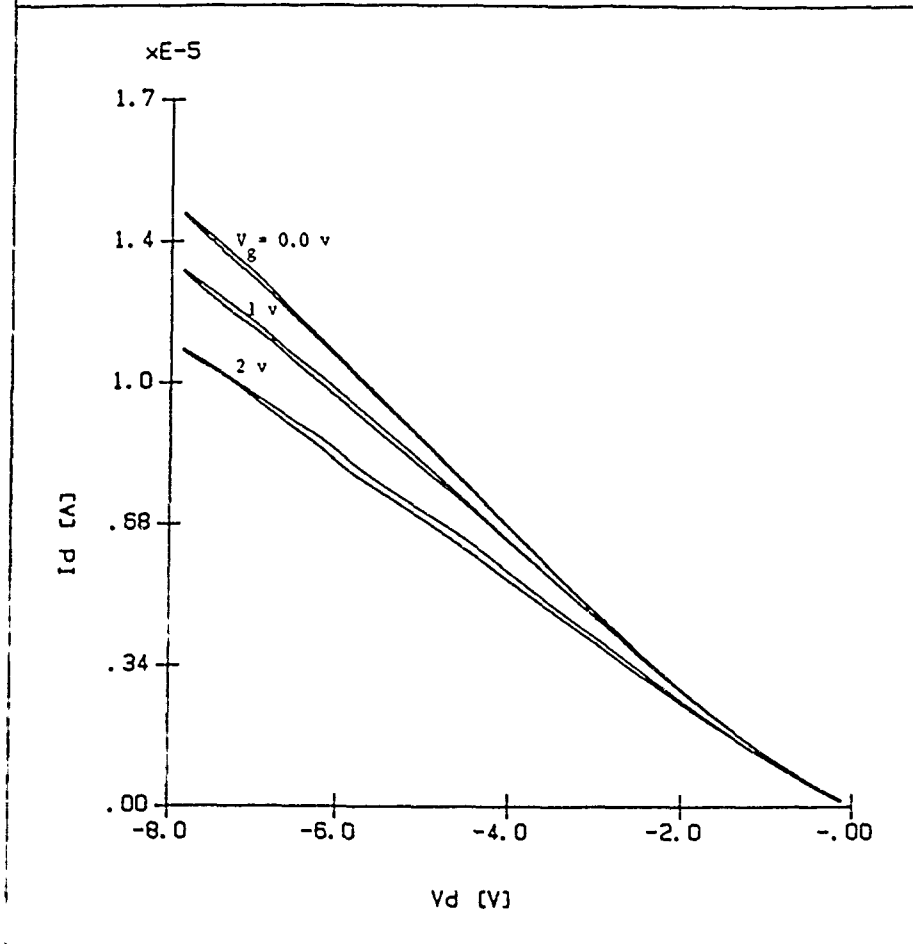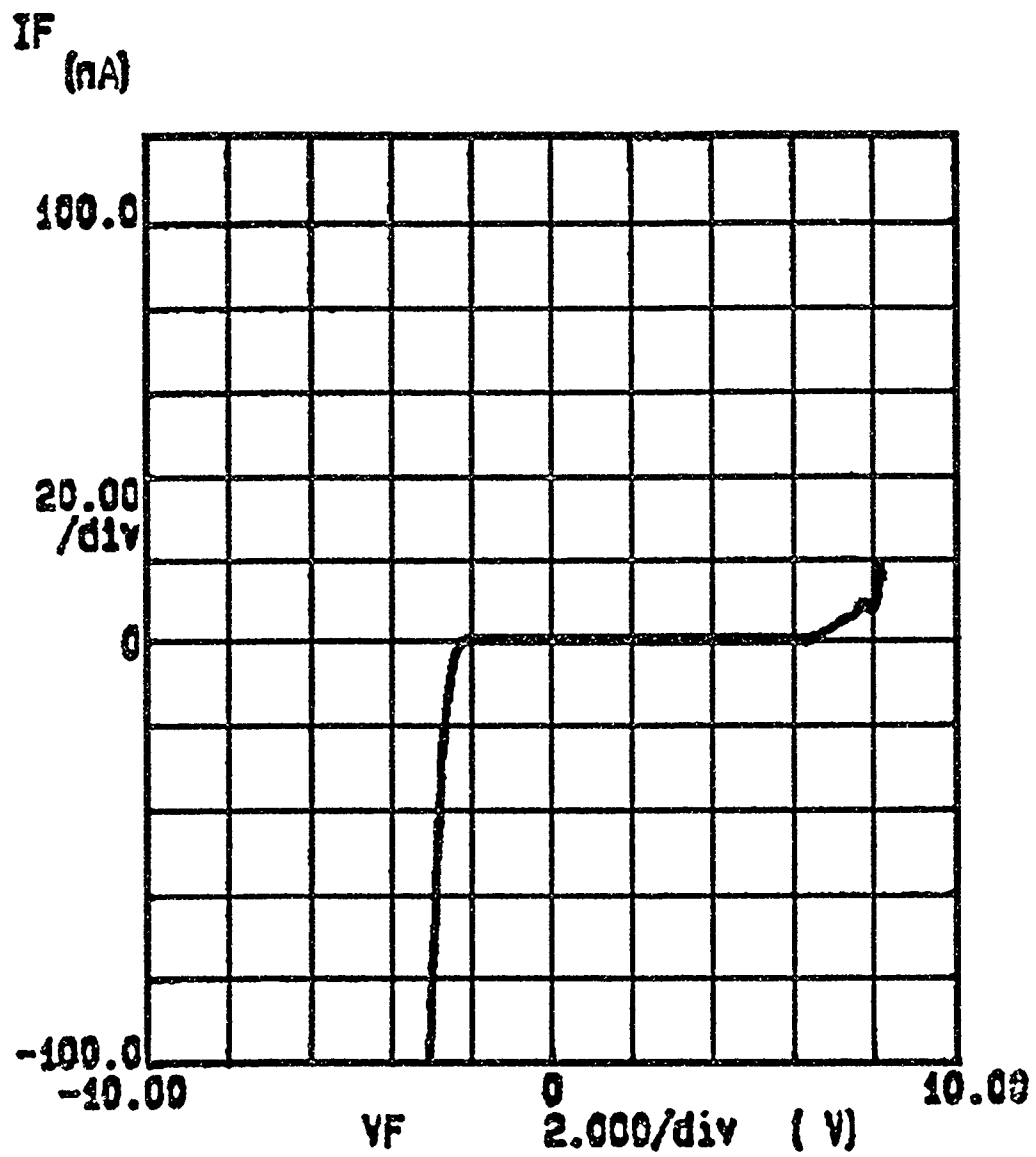
FIGURE 2.6.

FIGURE 2.7.
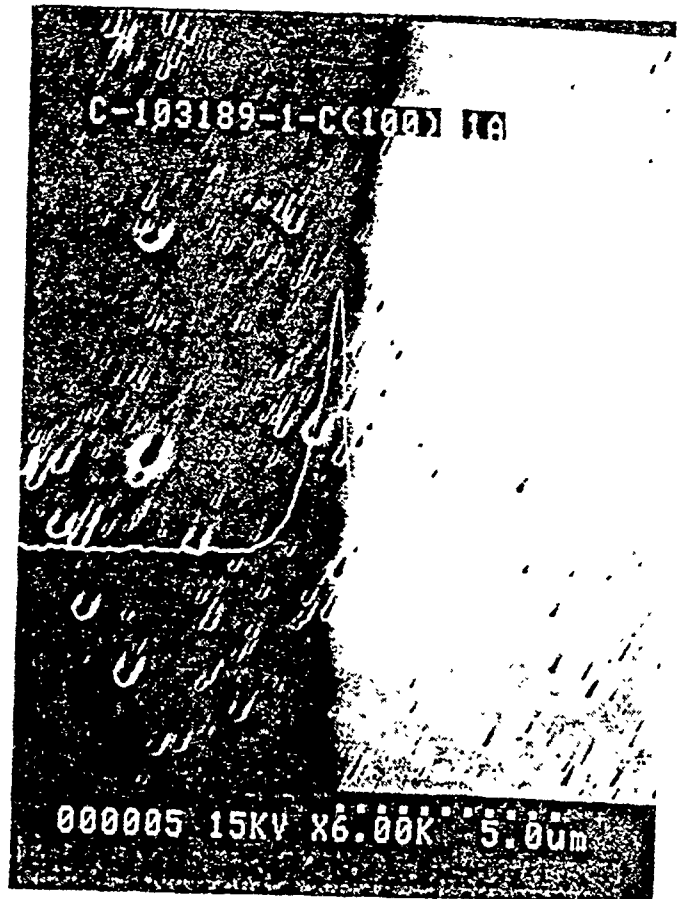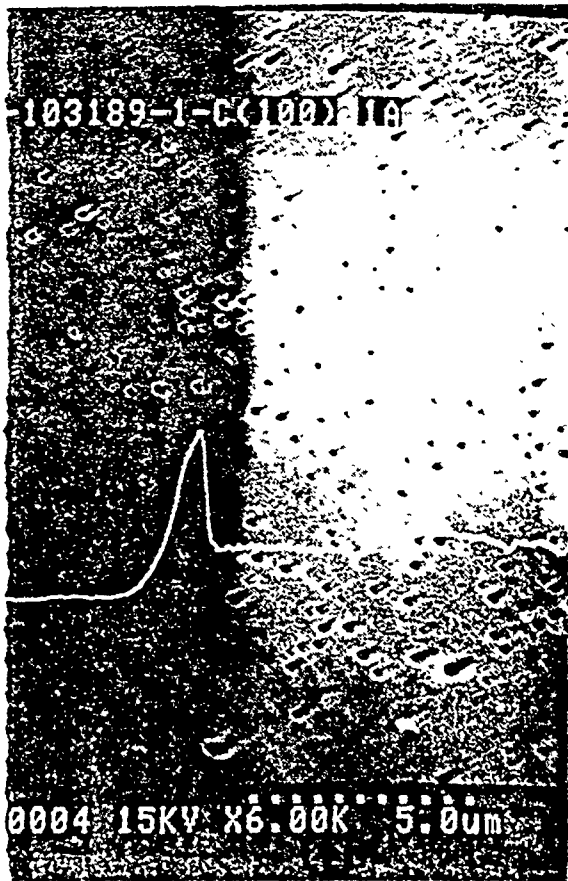
FIGURE 2.8.

3.0   PROGRESS IN ALE DEVELOPMENT

Work at Research Triangle Institute has also been focussing on the development of novel techniques for diamond deposition. Novel techniques are needed which will enhance the nucleation of diamond on non-diamond substrates.

Basically, conventional hydrocarbon processes (plasma or filament activated) are capable of depositing diamond. However, the nucleation on foreign substrates is highly three-dimensional with an extremely low nucleation density. This is probably a consequence of the extremely high surface energy of diamond. This results in a conglomeration of of the diamond into sparse nuclei where the surface energy is minimized. This phenomenum is probably enhanced by the growth of diamond under conditions whereby the substrate surface is hydrogen stabilized. This stabilization makes the surface less reactive to hydrocarbon radicals and promotes surface diffusion to the nuclei.

We have begun the development of alternative CVD technologies. principally the development of atomic layer epitaxy techniques. In beginning the development. we recognize that the control of the surface chemistry will be of paramount importance in any ALE scenario for diamond. It must both control the surface reactions and stabilize the surface as diamond. Much of our work this year has been dedicated to refinement of gas dosing and thermal desorptions techniques to allow investigation of hydrogen-halogen reactions on diamond surfaces. We are now in a position to begin those experiments after having proofed and refined the system through the study of hydrogen-halogen reactions on Si(100) surfaces.

In conjunction with the surface chemistry work, Research Triangle Institute continued its pioneering work in thermal CVD of diamond using halogens. The original work was reported in August 1989 in *Electronic Letters* was CF_4/F_2 homoepitaxy. Following the report from Rice University of heteronucleation using CH_4/F_2, we have begun addressing that system. This has involved reconfiguration of the reactor to progress to higher pressures and was proceeded by mass quadrupole analysis of the thermal reactions of CH_4 and F_2 in a hot graphite oven.

3.1 Thermal CVD of diamond

A new technique for diamond deposition was derived last year from work performed at Research Triangle Institute for the purpose of developing a diamond atomic layer epitaxy (ALE) process. While this technique is not an ALE process. it represents an important step away from plasma or filament assisted processes. With this technique, diamond is grown by passing a CF_4, F_2 mixture across a heated substrate (850 °C). The F_2 is decomposed at this temperature and can readily dissolve graphite from the growth surface allowing diamond sites to dominate the surface. CF_4 was added as the source gas for diamond deposition. Experiments with the CF_4/F_2 process have been limited by the need to pre-deposit carbon on the reactor walls for substantial amounts of time to avoid metal incorporation in the films. The metal contamination derives from fluorine-etch and vapor transport from the walls to the depositing film. The CF_4/F_2 process may indeed be convoluted by fluorine reactions with the hydrogenated carbon deposits on the walls of the reactor. Hydrogen transported

from the hydrogenated wall deposits may be playing a critical role in the process. Experiments with mixed fluorocarbons-hydrocarbons should yield insight into that process.

Recent work by Patterson at Rice University and previous work at Research Triangle Institute have shown that diamond deposition from a fluorine-based environment is possible. Patterson exploited the use of mixed fluorine-hydrogen chemistries (i.e., F_2 and CH_4) to form solid carbon through a proposed reaction of:

$$CH_4 + 2\,F_2 \rightarrow C_{(5)} + 4HF \tag{1}$$

The free energy of the reaction would be more exothermic than a corresponding hydrogen-based reaction involving CH_4 and H_2. The hot zone of the Patterson-type reactor operated between 700 and 950°C, and diamond growth occurred only in regions of the reactor where the temperature was between 250 and 750°C.

To gain insight into the fluorine-based process, we have performed a quadrupole mass spectroscopy of F_2/CH_4 gas interactions as a function of temperature. The work is performed in an UHV compatible chamber that is evacuated by a corrosive series, 1000 l/s turbomolecular pump. Gases are admitted into the chamber using mass flow controllers. The pressure in the chamber is maintained at 0.500 Torr for F_2 - CH_4 gas work described here. A heated graphite strip is enclosed in the chamber as well as a sample heater stage whereby growth attempts independent of the graphite strip heater can be assessed. The graphite heater is machined from a dense, fine-grain graphite and is not highly oriented pyrolytic graphite. A mass quadrupole operating at low emission (0.25 mA) is used to sample the gases exiting the reactor. By adjusting the

current through the graphite element, the reactions of F_2 and/or F with the densified graphite can be studied as a function of temperature. One advantage in using a graphite heater to study the F_2/CH_4 gas interactions is that reactions of fluorine with graphite has been previously studied, so there exists comparative information. A second advantage to the graphite heater is that it avoids questions of metal catalysis reactions.

Figure 3.1 shows the observed CF_3 mass counts in the reactor as a function of temperature. The main ionization product of CF_4 is CF_3. The CF_4 production is observed to decrease for temperatures in excess of $950\,^\circ C$. The temperature dependence is convoluted by the fact that there is a substantial temperature variation$\pm$ $100\,^\circ C$ across the graphite heater element. Upon introduction of CH_4 into the hot fluorine, the CF_4 production decreases. Fluorine interactions with the CH_4 is the gas phase will deplete the gas phase of fluorine, resulting in a lower incident flux of F atoms to the graphite surface, and a lower production rate of CF_4. This is the first evidence observed for $F_2 - CH_4$ gas interactions. Besides the reduction in CF_4 production, the introduction of CH_4 into the hot fluorine produces HF and C_2F_2H production. Figure 3.2 shows the production of those molecules as a function of the graphite temperature. The temperature dependence for the HF production is more pronounced than the temperature dependence for the C_2F_2H production. Both exhibit a maximum in production around $900\,^\circ C$.

This work suggests that the proposed reaction of Patterson. et al. for solid carbon production via equation (1) is basically correct. Our observations of (1) thermal atomic fluorine production, (2) gasification of graphite into CF_4, and the formation of HF and

26

C_2F_2H by-products, suggests that the reaction in equation (1) should be extended.

$$2F_2 \rightarrow^{700 \; °C} 4F + CH_4 \rightarrow C_{solid} + 4HF$$

$$4F_2 \rightarrow^{700 \; °C} 8F + 2CH_4 \rightarrow C_2H_2F_2 + 6HF$$

$$2F_2 + C_{graphite} \rightarrow^{500 \; °C - 700 \; °C} CF_4$$
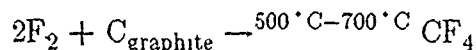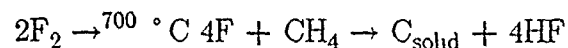
3.2 Hydrogen-Halogen Exchange Reactions

Using thermal mass desorption and LEED we have studied interactions of H, Cl_2. and F_2 with a silicon (100) surface, and exchange reactions of the gases with adsorbates on the silicon (100) surface. Thermal desorption spectra were measured for surfaces dosed with H, Cl_2, and F_2 singly and then for surfaces dosed first with a halogen and then atomic hydrogen. Finally, the reverse sequence was studied, with atomic hydrogen dosing and then the halogen exposure.

A W filament at approximately 2000 °C was used for the production of atomic hydrogen. Dose rate was set by measuring the chamber pressure, and dosing for a predetermined time. For all gases except atomic hydrogen, all filaments are turned off during dosing. After dosing the sample was moved in front of the quadrupole for thermal desorption. Dosing gases used included a 99.99% chlorine source. 99.999% hydrogen, and 2.0% fluorine in helium. All thermal desorption spectra were taken at a heating rate of 5 °C/sec.

Halogen coverages were not measured directly. Instead. the samples were dosed for a fixed period of time with a series of increasing pressures. After each halogen dose a

thermal desorption spectrum was taken and the intensity of the SiCl or SiF$_2$ peak noted. As the pressure was increased in the desorption series a saturation in the intensity of the desorbed halo-silanes was seen. This saturation occurred at a total dose of 120×10^{-6} Torr-seconds for chlorine and at a total dose of 90×10^{-6} Torr-seconds for the 2 % F$_2$ in He gas mixture.

Figures 3.3 and 3.4 show the effects of atomic hydrogen dosing on the thermal desorption spectra of a chlorine dosed sample. Samples held at 25 °C were first dosed with molecular chlorine and then with atomic hydrogen at varying pressures. The figures track desorbing H$_2$, and SiCl, as a function of total hydrogen dose. In the hydrogen desorption spectra, Figure 3.3, characteristic peaks appear at 425 °C and 540 °C after dosing with atomic hydrogen. These peaks are commonly referred to in the literature as the β_2 and the β_1 peaks respectively. LEED measurements after the hydrogen dosing and prior to desorption confirm the transformation from a 2x1 structure to a 1x1 structure. Figure 3.4 follows the SiCl desorption peak as a function of total dose of atomic hydrogen. We observe that as the total hydrogen dose increases the amount of SiCl subsequently desorbed decreases.

Figure 3.5 shows a plot of normalized peak counts for SiCl desorption. Data from two groups of samples are shown: samples that were dosed with chlorine and then dosed with atomic hydrogen at an elevated temperature, and for samples dosed with chlorine and annealed at an elevated temperature without hydrogen dosing. For the samples not receiving hydrogen dosing we see little evidence of SiCl desorption until the 600 °C anneal indicating that the SiCl is relatively stable below the desorption

temperature. In contrast, hydrogen extracts an increasing amount of chlorine as the temperature is increased. In general we find that annealing at a given temperature during hydrogen dosing removes peaks in the spectra that had a desorption temperature lower than the annealing temperature. For example, after annealing at 200°C the β_2 hydrogen peak remains. However, annealing at 400°C removes the β_2 peak. A similar effect was observed for HCl and SiCl desorption peaks.

The results for fluorine are quite similar to what was seen for the chlorine work. The major difference is that SiF_x species desorb at a lower temperature than $SiCl_x$ species. Masses monitored for these experiments were 2, 19, 66, 85, and 86, which corresponds to H_2, F, SiF_2, SiF_3, and SiF_3H, respectively. Figures 3.6 and 3.7 show a series of thermal desorption spectra where the sample, held at 25°C, was first saturated with molecular fluorine, and then dosed with atomic hydrogen at a series of increasing total doses. We see a steady decline in the SiF_2 counts as the total hydrogen dose is increased.

Two additional experiments were performed. In the first, samples were dosed with atomic hydrogen to saturation and then exposed to F_2 at 25°C. No evidence of SiF_x desorption was seen after this dosing. In the second experiment, samples were dosed with molecular fluorine and then dosed with molecular hydrogen. Again no evidence of exchange was seen. Detailed discussion of these results have been included in the third quarterly report.

Our findings are that atomic hydrogen will remove both chlorine and fluorine from a silicon (100) surface. Molecular hydrogen in contrast is ineffective at displacing

these halogens. Evidence suggests, at least in the case of chlorine, that removal occurs via the formation of HCl rather than a volatile $SiCl_xH_y$ species. Furthermore the hydrogen/chlorine removal is found to be effective up to the desorption temperature of the $SiCl_x$ species. In spite of the favorable energetics there was no evidence that either molecular chlorine or molecular fluorine would remove hydrogen from the silicon surface at 25 °C.

During the fourth quarter we resolved problems associated with heating a single crystal diamond sample. Efforts to bond the diamond to a silicon heater strip proved unreliable and were abandoned in favor of a tantalum strip heater to which the diamond is wired. The diamond, a 5mm x 5mm (100) crystal, is held firmly against the tantalum strip by 2-.127mm tantalum wires. The strip consists of a 2.5mm x 25mm x .5mm tantalum foil. Temperatures in excess of 1500 °C can easily be achieved with this arrangement. A small amount of graphite paste is used to provide increased thermal conductivity between the diamond and the heater. The temperature of the sample is monitored via a W3%Re-W25%Re thermocouple spot-welded to the tantalum strip in close proximity to the diamond.

Several improvements were made to the surface chemistry facility during this quarter. Since hydrogen desorption from diamond occurs at a much higher temperature than on silicon more outgassing is seen from chamber fixtures and system improv ments were made to further isolate the quadrupole mass spectrometer from the main chamber. We can now maintain a pressure differential of more than three orders of magnitude between the chamber in which the sample is heated and the quadrupole

which samples gas desorbing from the diamond surface. We expect this new arrangement to substantially improve sensitivity to desorbing species. Calibrated dosers were added to the main chamber during the fourth quarter. With these in place we can now deliver a calibrated quantity of gas in a uniform manner to the diamond surface.

CF$_4$ Production
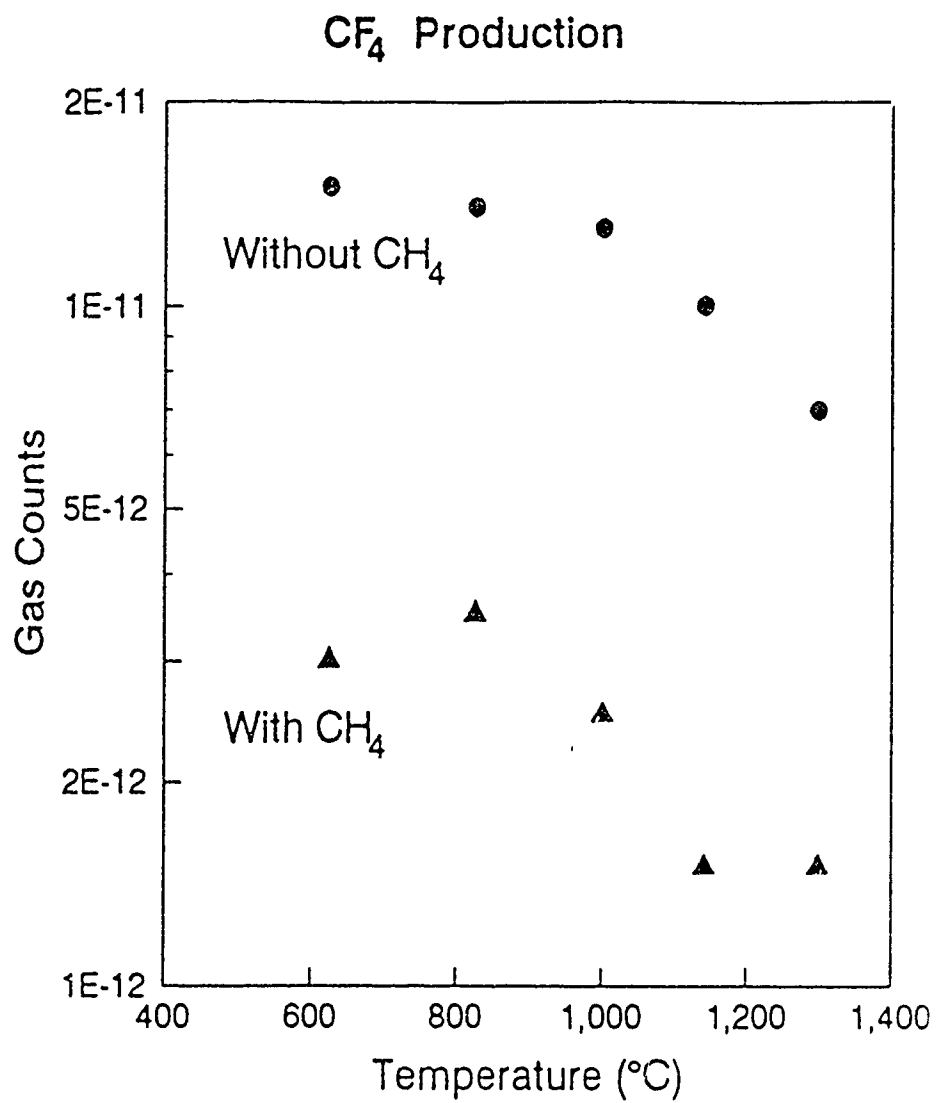
FIGURE 3.1.

F_2 - CH_4 By-Products
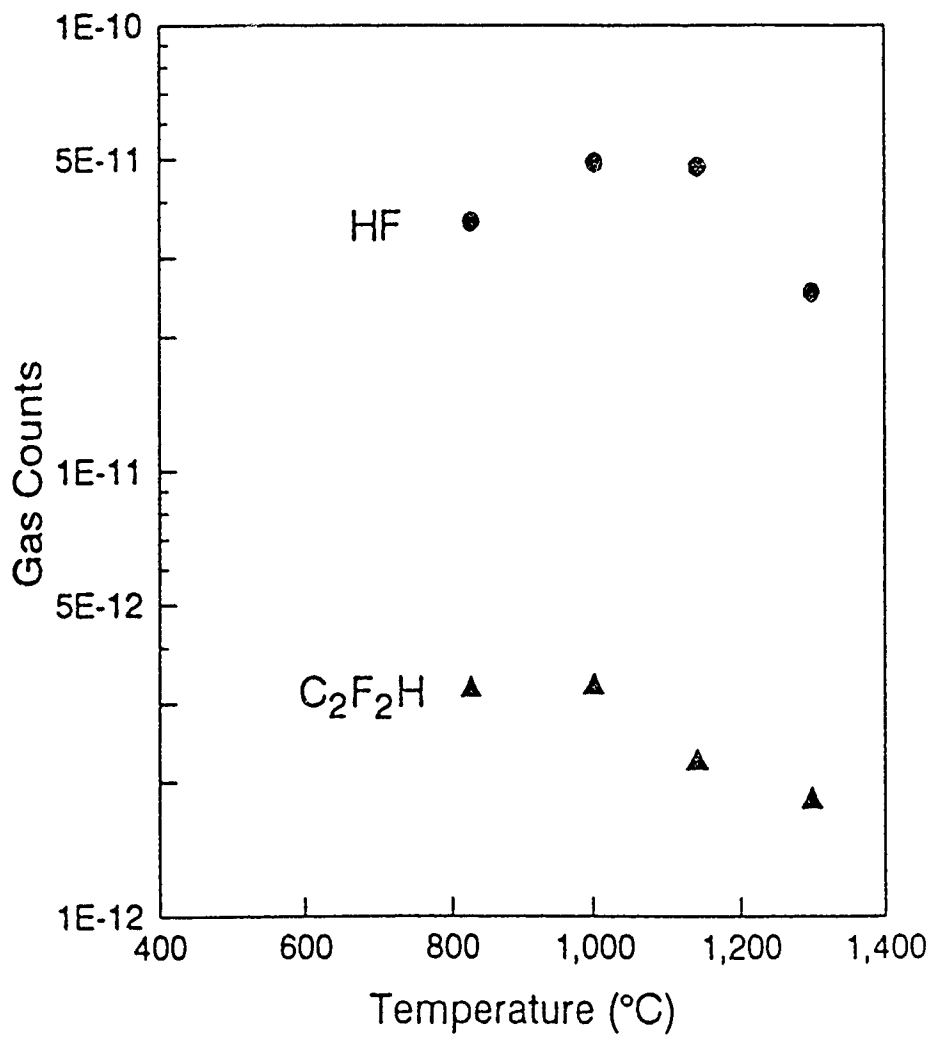
FIGURE 3.2.

Hydrogen Desorption

Chlorine Dosing
120 seconds

Hydrogen
Dosing
Pressure

5E-6
2.5E-6

1E-6
5E-7

1E-7

Counts (Arb. Units)

Temperature (°C)
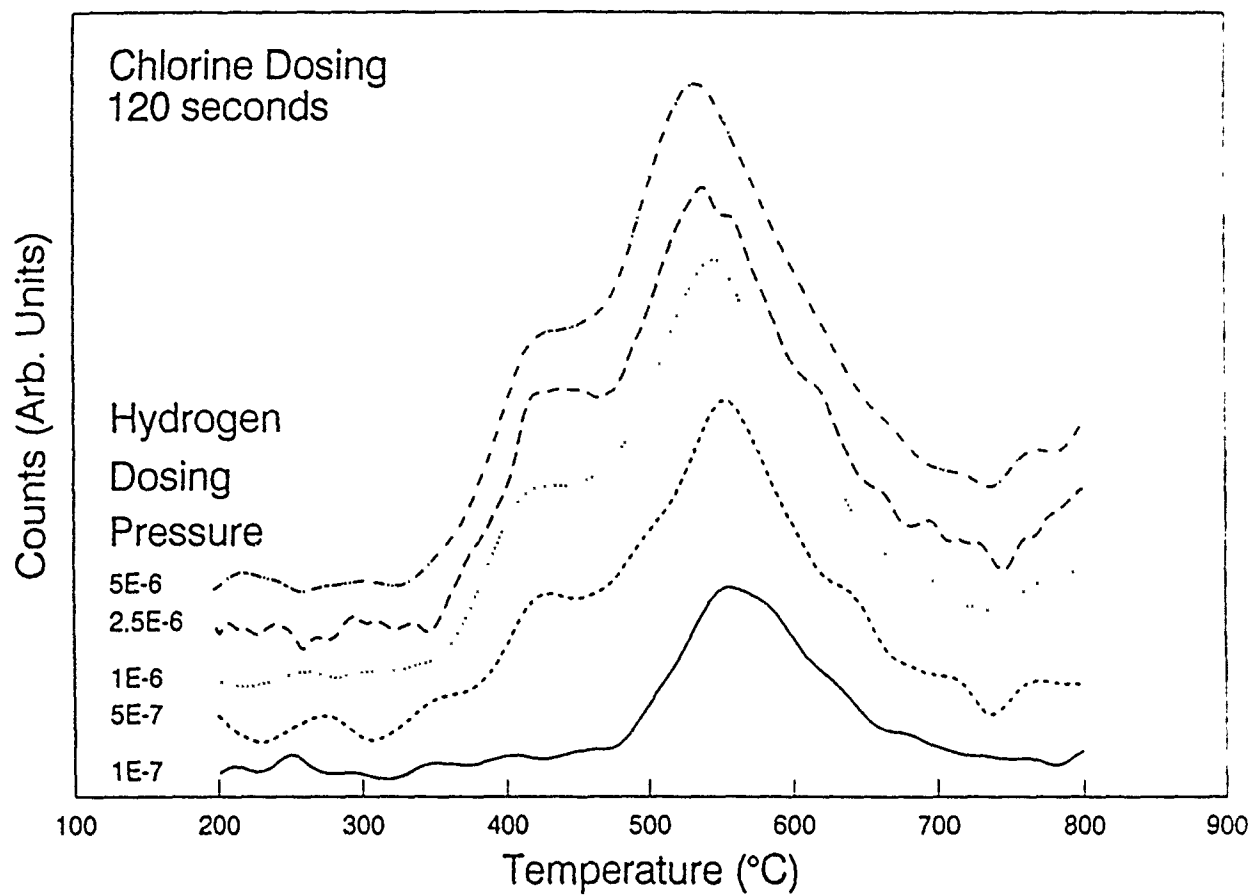
FIGURE 3.3.

SiCl Desorption
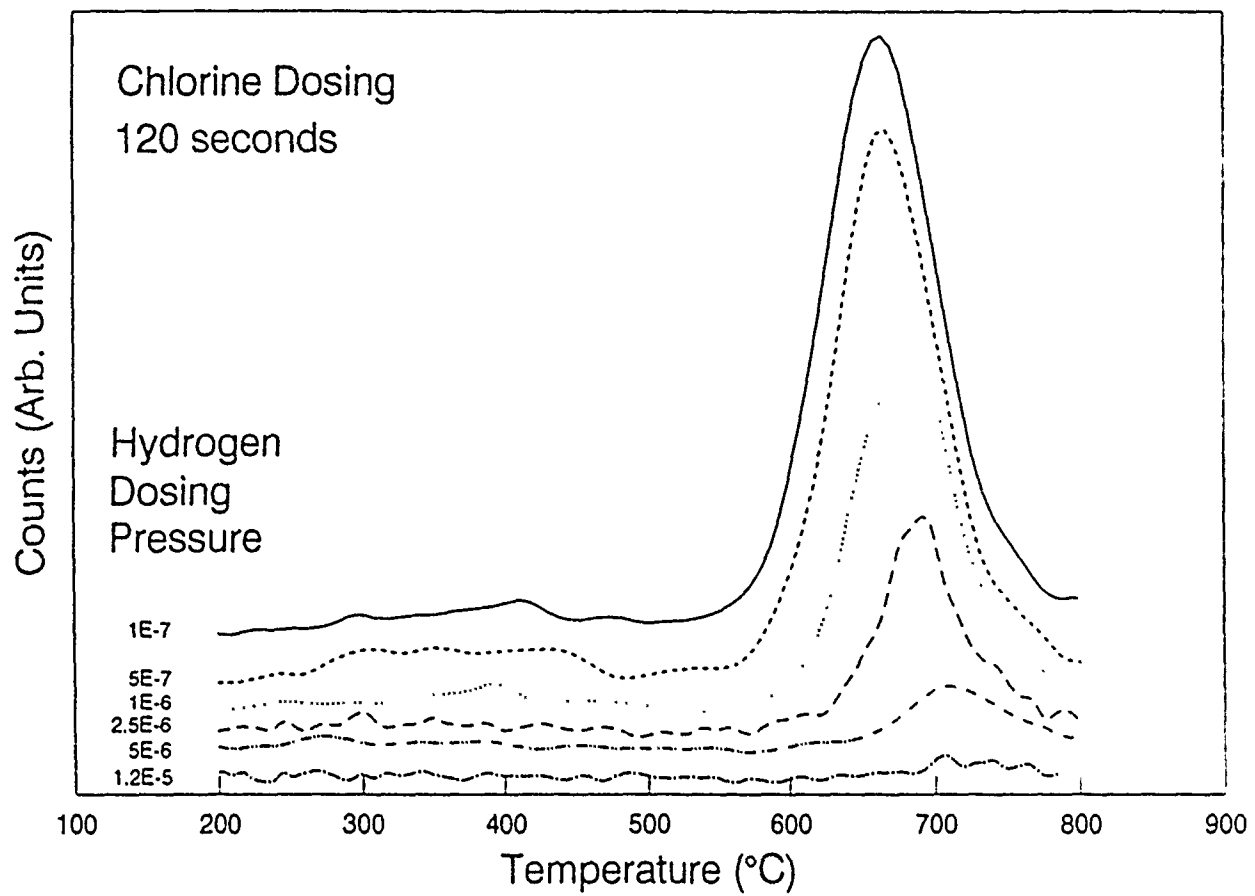
FIGURE 3.4.

SiCl Peak Heights

FIGURE 3.5.

Hydrogen Desorption

Fluorine Dosing
135 Seconds
7E-7 Torr
2% F_2 / He

Counts (Arb. Units)

Hydrogen
Dosing
Pressure

1.1E-6

1E-7

0

Temperature (°C)
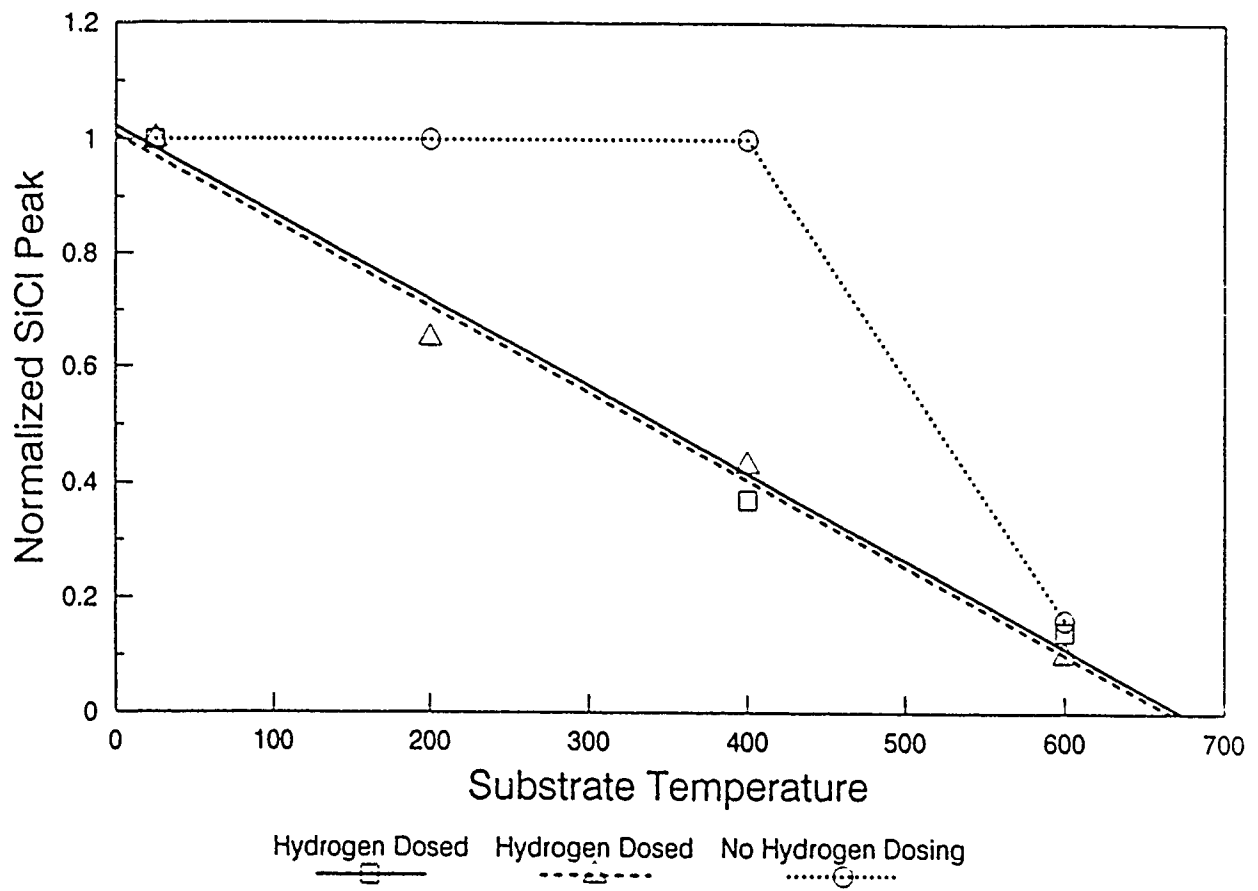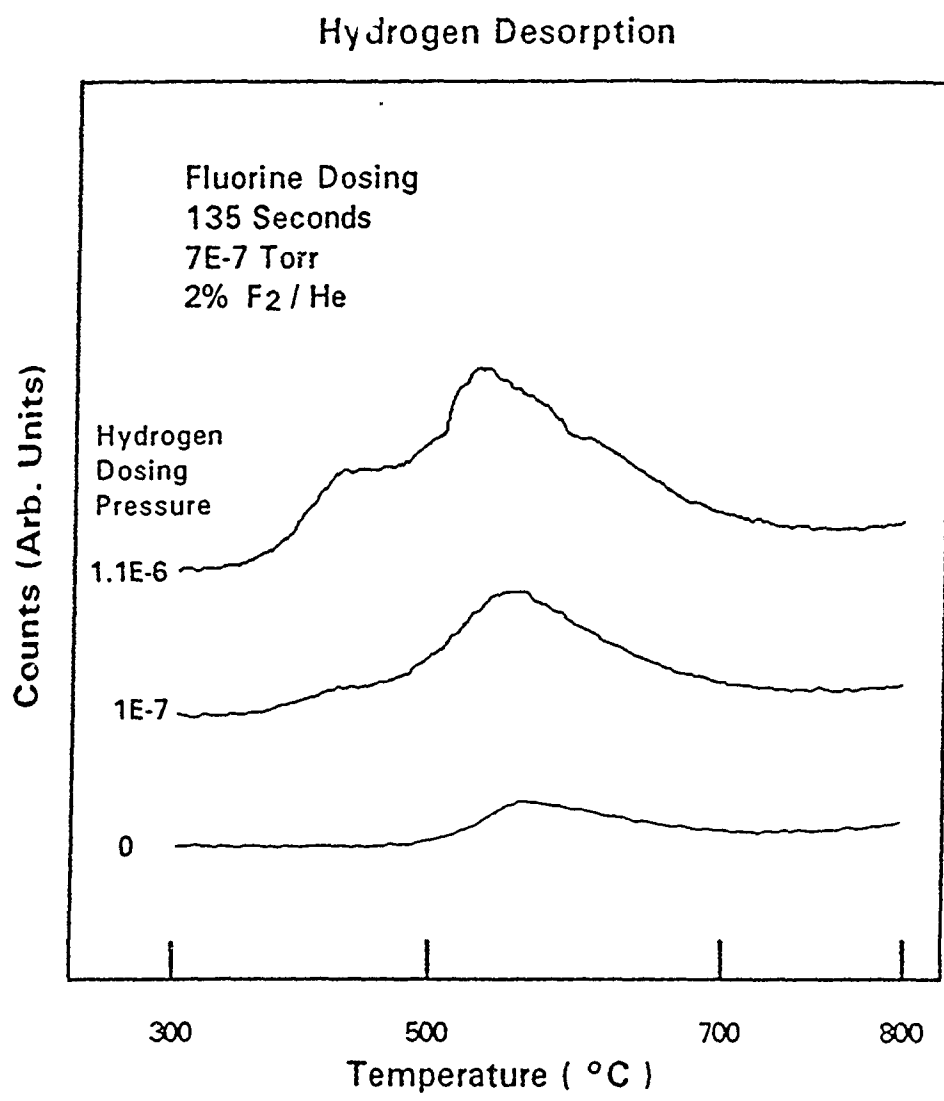
FIGURE 3.6.

SiF$_2$ Desorption

Fluorine Dosing
135 Seconds
7E-7 Torr
2% F$_2$ / He

Counts (Arb. Units)

Hydrogen
Dosing
Pressure

0

1E-7

1.1E-6

Temperature (°C)

300   500   700   800

FIGURE 3.7.

38
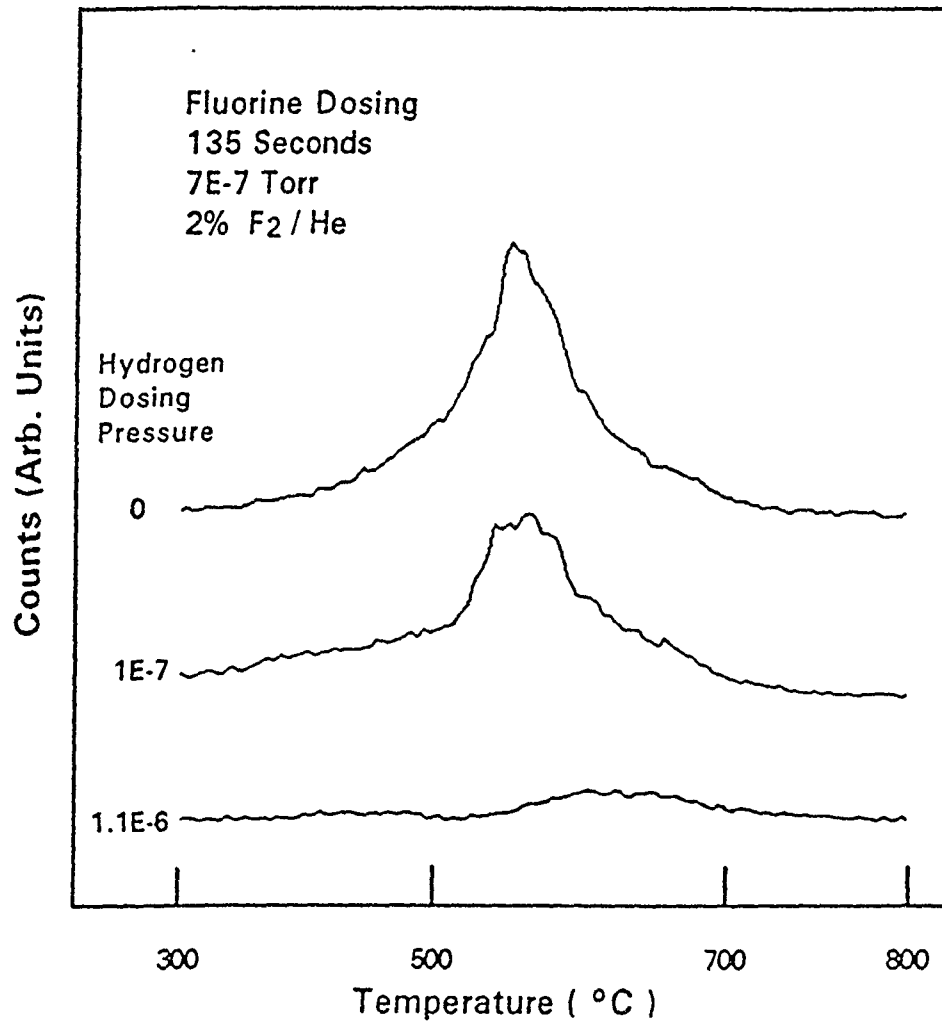
4.0 METAL SUBSTRATE DEVELOPMENT AND HETERONUCLEATION STUDIES

Research in a previous phase of this program has already demonstrated the ability to prepare and polish Ni single crystals for subsequent growth of epitaxial metal layers. Additionally, molecular beam epitaxy (MBE) has been used to grow Ni_xCu_{1-x} epitaxial films of different compositions and, hence, lattice parameters. As the Ni and Cu lattice parameters straddle the lattice parameter of diamond, this approach to substrate development for diamond heteroepitaxy was utilized to engineer an exact lattice match with the diamond $[a_o (Ni_{0.82}Cu_{0.18}) \simeq 3.567$ Å $\simeq a_o$ (Diamond) at T = 700 °C]. This capability already exists.

Substrate development this year has built upon the available metals MBE expertise by investigating the modification of surface chemistry while maintaining near-lattice-matching to diamond. In particular, the deposition of Mo onto Ni(100) was explored. The technical approach for this was to deposit an ultra thin layer of a highly reactive refractory metal (strong carbide forming element) on a Ni(100) surface that would be epitaxial and, possibly, pseudomorphic. Although bulk Mo is body-centered cubic with a lattice parameter of a_o(Mo) = 3.1463 Å, the potential still exists to modify the surface of a Ni(100) crystal chemistry while maintaining near lattice matching to diamond.

Ar^+ sputter-cleaned annealed samples were transferred from an UHV integrated processing system into the metal MBE growth chamber of the integrated processing facility. The growth rate was controlled by a quartz crystal oscillator and was typically

39

0.2 Å- sec^{-1}. The samples were characterized without breaking vacuum by LEED, XPS, and AES. The variation of the AES intensities with increasing film thickness has been used to determine the mode of growth at 200°C. Figure 4.1 shows the first derivative Auger intensities of the Mo MNN (186eV) and Ni LMM (61eV) transitions from the Mo/Ni(100) surface as a function of Mo film thickness. The exponential intensity indicates a layer by layer growth mechanism.

In order to obtain an epitaxial relationship between the deposited Mo films and the Ni substrate, the growth temperature was increased. Growth of ultrathin ($\sim$ 20 Å) Mo on Ni(100) resulted in a well-defined LEED pattern at 550°C. These patterns are similar to the diffraction pattern of the Ni(100) substrate. The same tendency was observed for a thicker film ($\sim$ 250 Å Mo). However, AES of Mo films of up to 500 Å thickness grown at 550°C on Ni(100) clearly show the Ni LMM (61eV) transition which has a very low escape depth ($<$ 10 Å). The source of this phenomenon could be: (a) incomplete coverage, (b) intermetallic or alloy formation during growth, or (c) a persistent thin Ni coverage on the growing Mo film. SEM reveals that the growth morphology is clearly 3-dimensional. High-resolution AES (HRAES) measurements utilizing an electron beam current of $\sim$ 0.8 nA at a beam size of $\sim$ 0.1 diameter reveal bare Ni channels in between the 3-dimensional Mo deposit. HRAES data taken while focusing on the surface of a Mo island still shows the presence of Ni LMM (61 eV and 848 eV) signals. However, after brief sputtering ($<$ 15 Å) these signals vanish, restoring a clean Mo surface. This excludes intermetallic/alloy formation during growth with the possible exception of the Mo/Ni interfacial region. Therefore, the source of

the Ni LMM peaks on the as-grown surface of the Mo islands is the coverage of these islands by Ni atoms during all stages of nucleation and growth processes.

In summary, the growth of thin Mo layers on Ni(100) and multilayer Mo-Ni heterostructures has been investigated. At 200°C, polycrystalline, uniform, and topographically featureless Mo on Ni(100) films are formed. In contrast, growth of Mo on Ni(100) at 550°C proceeds by the Volmer-Weber mechanism. This precludes the fabrication of contiguous epitaxial Mo-Ni multilayer structures of small period ($<$ 1000 Å) using conventional electron-beam MBE. Finally, annealing experiments performed on Mo/Ni(100) heterostructures deposited at 200 °C, show an onset of interdiffusion at $\sim$550 °C and, simultaneously, a unique reconstruction of the surface.

Attempts were made to grow diamond on a Mo-terminated Ni(100) crystal. An ultrathin layer ($\sim$ 20 Å) of Mo was grown on Ni(100) at 200°C by MBE using the method described above. Based on results described above, it was believed that once the Mo/Ni(100) structure was raised to the diamond growth temperature of $\sim$ 600°C, interdiffusion would create a surface structure and chemistry similar to that observed previously. Due to the need to perform other tasks on this program, the diamond reactor on the integrated processing system was not available for in-vacuo transfer of the Mo/Ni(100) substrate to a diamond CVD system. Hence, an air transfer was utilized. The PECVD diamond growth was done at a temperature of $\sim$ 600°C; using a mixture of CO, CH_4, and H_2; at a pressure of 1 Torr. Figure 4.2 shows SEM results from this run. Notice the difference in the diamond nucleation density between the Mo/Ni(100) region and the "bare" Ni(100) region (this region did not receive Mo depo-

41

sition because it was under the mask). Somewhat surprisingly, the nucleation density of diamond is substantially greater on the "bare" Ni(100) surface. Although this appears to suggest that an ultra-thin Mo interlayer does not promote diamond nucleation, we are of the opinion that this experiment is not definitive. It is most probable that all the ~ 20 Å Mo was oxidized during the air transfer to the diamond reactor.
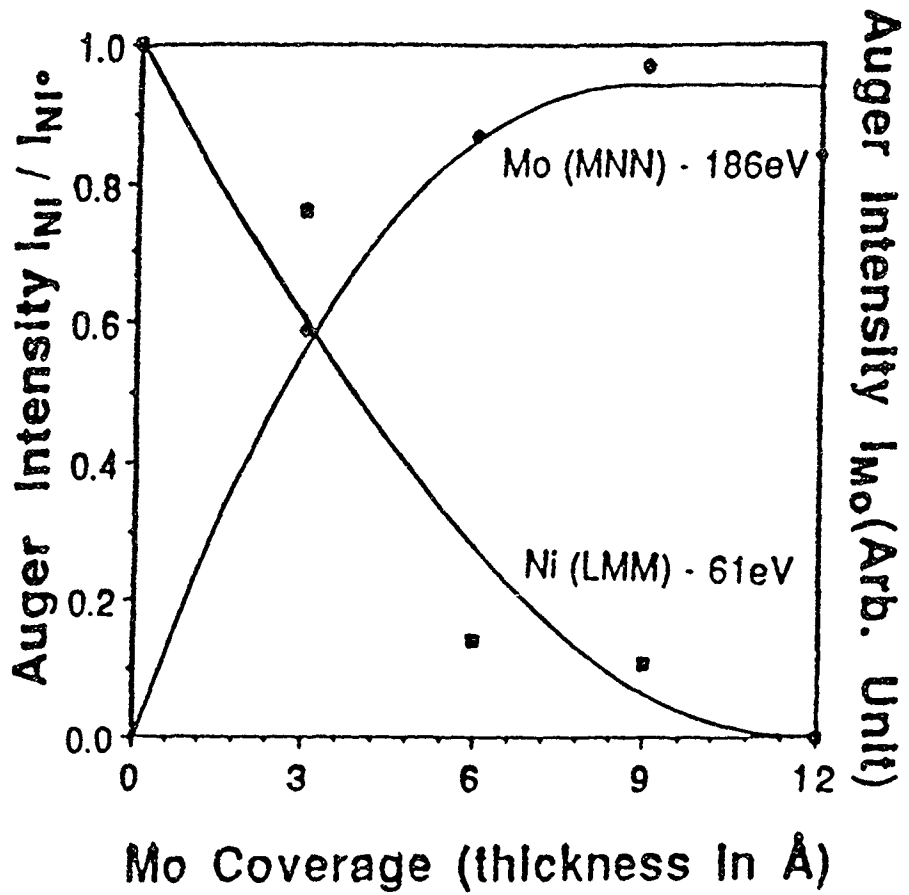
FIGURE 4.1.
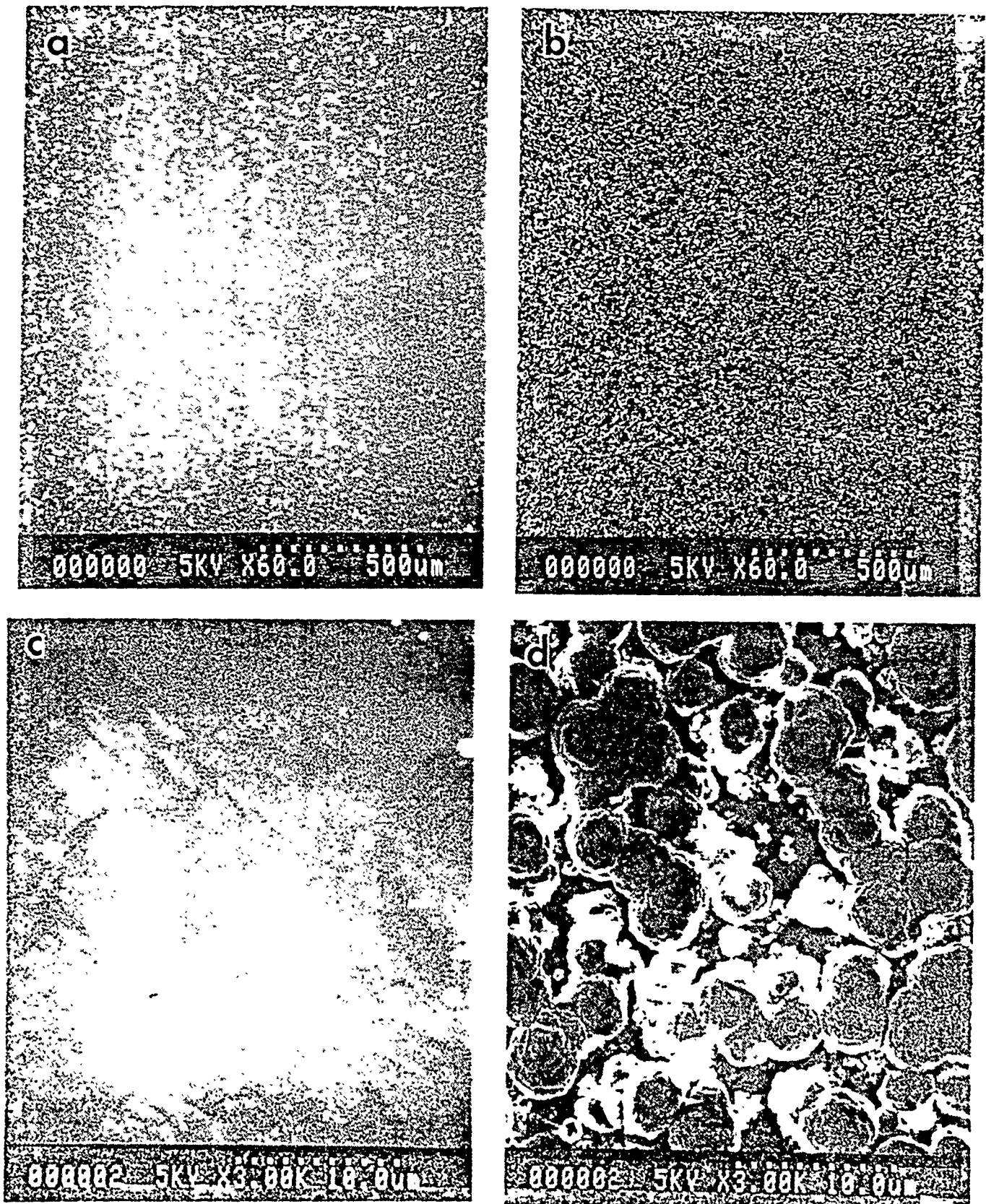
FIGURE 4.2.   SEM micrographs from diamond deposition on Mo/Ni(100) hetero-structure: (a & b) low magnification comparing Mo-terminated region with bare Ni; (c & d) higher magnification comparing Mo-terminated region with bare Ni.

44

5.0 H_2/CF_4 PLASMA-ASSISTED CVD

Direct deposition of polycrystalline diamond films on Si(100) without surface pretreatment

R.A. Rudder, G.C. Hudson, J.B. Posthill, R.E. Thomas, and R.J. Markunas

Research Triangle Institute, Research Triangle Park, North Carolina 27709-2194

Dense nucleation of small-grain polycrystalline diamond films on Si(100) substrates has been accomplished without the use of any surface pretreatment such as abrasive diamond scratching, surface oil treatments, or diamond-like carbon predeposition. The depositions occurred in a low pressure rf plasma assisted chemical vapor deposition system using mixtures of CF_4 and H_2. Films deposited at 5 Torr and 850°C on as-received silicon wafers show dense nucleation, well-defined facets, and crystallites which ranged in size from 500 to 10,000 Å. X-ray photoelectron spectroscopy and electron energy loss show the films to be diamond with no major impurity and no detectable graphitic component Raman spectroscopy shows a pronounced 1332 cm^{-1} line accompanied with a broad band centered about 1500 cm^{-1}.

Growth of polycrystalline diamond from the gas phase at pressures near and below atmospheric pressure has been well-documented and reported.[1-7] A variety of techniques have been developed for chemical vapor deposition of diamond. These techniques have involved microwave plasmas, rf plasmas, hot filaments, arc-jets, rf-plasma torches, and acetylene torches. Typically, the source gasses used for diamond deposition have been hydrogen with dilute concentrations of hydrocarbon. It has been observed that (1) diamond nucleates well on itself and cubic boron nitride, (2) scratching of non-diamond surfaces with diamond abrasive enhances the diamond nucleation, and (3) diamond deposition without surface pretreatments such as scratching, oiling, or diamond-like carbon deposition does occur but at a much reduced nucleation rate. Without the surface pretreatments, deposition of thin continuous diamond films is not possible. Consequently, applications requiring thin continuous diamond layers have not been realized.

In this letter, we report on a technique for the deposition of diamond onto Si substrates without any pre-treatment of the wafer prior to its insertion into the growth reactor. The process has potential application in the deposition of diamond for heteroepitaxial growth, tool coatings, and optical coatings whereby dense nucleation is needed to promote epitaxial registration, chemical adherence, and optical transmission, respectively. More fundamentally, understanding the chemical process differences between diamond deposition between traditional CH_4 in H_2 plasmas which do not promote nucleation and the CF_4 in H_2 plasmas used in the present work which do promote diamond nucleation may permit the mechanisms of diamond hetero-nucleation to be elucidated.

The dense nucleation of polycrystalline diamond was accomplished in a low-pressure rf-plasma assisted chemical vapor deposition system. A schematic of the system is is shown in Figure 1. The reactor consists of a inductively coupled plasma tube vacuum pumped by a 1000 l/s turbomolecular pump. The plasma tube is a water cooled quartz jacket of $\sim$ 50 mm on the inside diameter. The quartz tube walls have been thoroughly covered with carbon deposition from previous diamond depositions using 1% CH_4 in H_2 discharges. The plasma is maintained by a 1-3 kW rf generator at 13.56 MHz. The samples are located on a graphite susceptor just beneath the rf coils. The system is equipped with a quadrupole mass spectrometer for sampling of gas flux from the plasma tube.

During deposition, the pressure was maintained at 5.0 Torr using 25 sccm of H_2 and 2 sccm of CF_4 pumped through an automatic control butterfly valve. The process gasses are exhausted into the turbomolecular pump. The samples were maintained at $\sim$ 850 °C using both inductive heating of the graphite susceptor from the rf coils and radiative heating of the susceptor from a graphite resistive heater. The plasma is maintained for the duration of the growth via inductive coupling of approximately 2000 W from the rf generator. The deposition time was 3 hrs for the samples reported herein. Monitoring of the gas flux from the plasma tube during deposition shows that the parent gas mix of CF_4 and H_2 is converted into HF and C_2H_2. No fluoromethane groups were observed.

Upon removal from the reactor, films showed dense nucleation of diamond over the unscratched Si surfaces. Scanning electron microscopy (SEM) micrographs from sample #1 are shown in Figure 2 At lower magnification, there is some thickness non-uniformity to the deposited layer. This may be a conse-

quence of diamond nucleation having occurred locally at different times after initiation of the discharge. At higher magnification, all features show well-defined facets with a broad distribution in grain size. Figure 2(d) shows the cleaved cross-section micrograph of sample #1. The diamond film is $\sim$ 1 μm in thickness. The cross sectional micrograph also shows that the silicon/diamond interface is non-planar suggesting that the Si surface was chemically etched prior to diamond nucleation and growth. Etching of the silicon surface could have occurred due to production of atomic fluorine from plasma dissociation of the CF_4. SEM micrographs of two other samples are shown in Figure 3. These samples were also deposited with a 8% CF_4 in H_2 gas mixture. The surface topography and crystallite size vary from sample to sample, but nearly the entire surface of the as-received silicon wafers show dense diamond nucleation.

Chemical determination of the films was accomplished with x-ray photoelectron spectroscopy (XPS). The XPS shows principally carbon present with some oxygen contamination probably from air transfer from the deposition system to the XPS unit. It is significant to note that no Si was observed in the films. It is interesting to note that no fluorine was observed. One might expect that the deposition of diamond from a fluorocarbon source would result in fluorine termination of the growth surface. At the growth temperatures of 850 °C employed in this work, work by Freedman and Stinespring[8] have shown that fluorine does not reside on a diamond (100) surface. Furthermore, in the atomic hydrogen environment produced by the high power rf discharge, any surface fluorine is energetically favored to be extracted from the surface via the formation of HF. Electron energy loss shows the surface of the film to be diamond.

The bulk and surface plasmons of diamond are observed. The graphitic plasmon (6 eV from the primary beam) was not observed. Characteristic Raman spectra are shown in Figure 4 for the samples #1 and #3. The Raman spectrum from each of the samples shows a clear 1332 cm^{-1} diamond longitudinal optical (LO) phonon. and each spectrum shows a broad feature around 1500 cm^{-1}. The broad feature is associated non-diamond material perhaps residing between the grains.

In conclusion, a plasma based process involving H_2/CF_4 which promotes dense nucleation and growth of polycrystalline diamond films on as-received Si wafers has been demonstrated. Mass spectroscopy of the gasses downstream from the plasma tube show that the H_2/CF_4 mixture is converted to HF and C_2H_2 with no detection of any fluoromethanes. The layers were characterized and determined to be diamond by Raman spectroscopy, x-ray photoelectron spectroscopy, and electron energy loss. SEM observations show the grain size to vary from 500 to 10,000 Å. Without the necessity of surface pretreatments for the growth of diamond, it is anticipated that this technique will find broad application in heteroepitaxial studies, optical coatings, tool coatings, and other areas.

References

1. B. Derjaguin and V. Fedoseev, Russ. Chem. Rev. 39, 783 (1970).

2. S. Matsumoto, Y. Sato, M. Kamo, and N. Setaka, Jpn. J. Appl. Phys. 21, 183 (1982).

3. Y. Hirose and Y. Teresawa, Jpn. J. Appl. Phys. 25. L51 (1986).

4. M. Nakazawa, T. Nakashima, and S. Seikai, Appl. Phys. Lett. 45. 823 (1984).

5. M. Kamo, Y. Sato, S. Matsumoto, and N. Setaka, J. Cryst. Growth 62. 642 (1983).

6. S. Matsumoto, M. Hiro, and T. Kobayashi, Appl. Phys. Lett. 51, 737 (1987).

7. K. Kurihara, K. Sasaki. M. Kawarada, and N. Koshiro, Appl. Phys. Lett. 52, 437 (1988).

8. Andrew Freedman and Charles D. Stinespring, Appl. Phys. Lett. 57, 1194 (1990).

Figure Captions

Figure 1.   Schematic of low-pressure rf-plasma assisted chemical vapor deposition system.

Figure 2.   Scanning electron micrographs of sample #1: (a), (b), (c) are progressively higher magnification views of the polycrystalline diamond surface; (d) is a micrograph of a cleaved cross-section showing some interfacial roughness between the diamond layer and the silicon surface.

Figure 3.   Scanning electron micrographs of samples #2 and #3: (a) and (b) are different magnifications of the polycrystalline diamond surface for sample #2; (c) and (d) are different magnifications of the polycrystalline surface for sample #3.

Figure 4.   Raman spectra from polycrystalline diamond deposition on as-received silicon surfaces: (a) is the spectrum from sample C-113090-1 and (b) is the spectrum from sample C-120790-1.
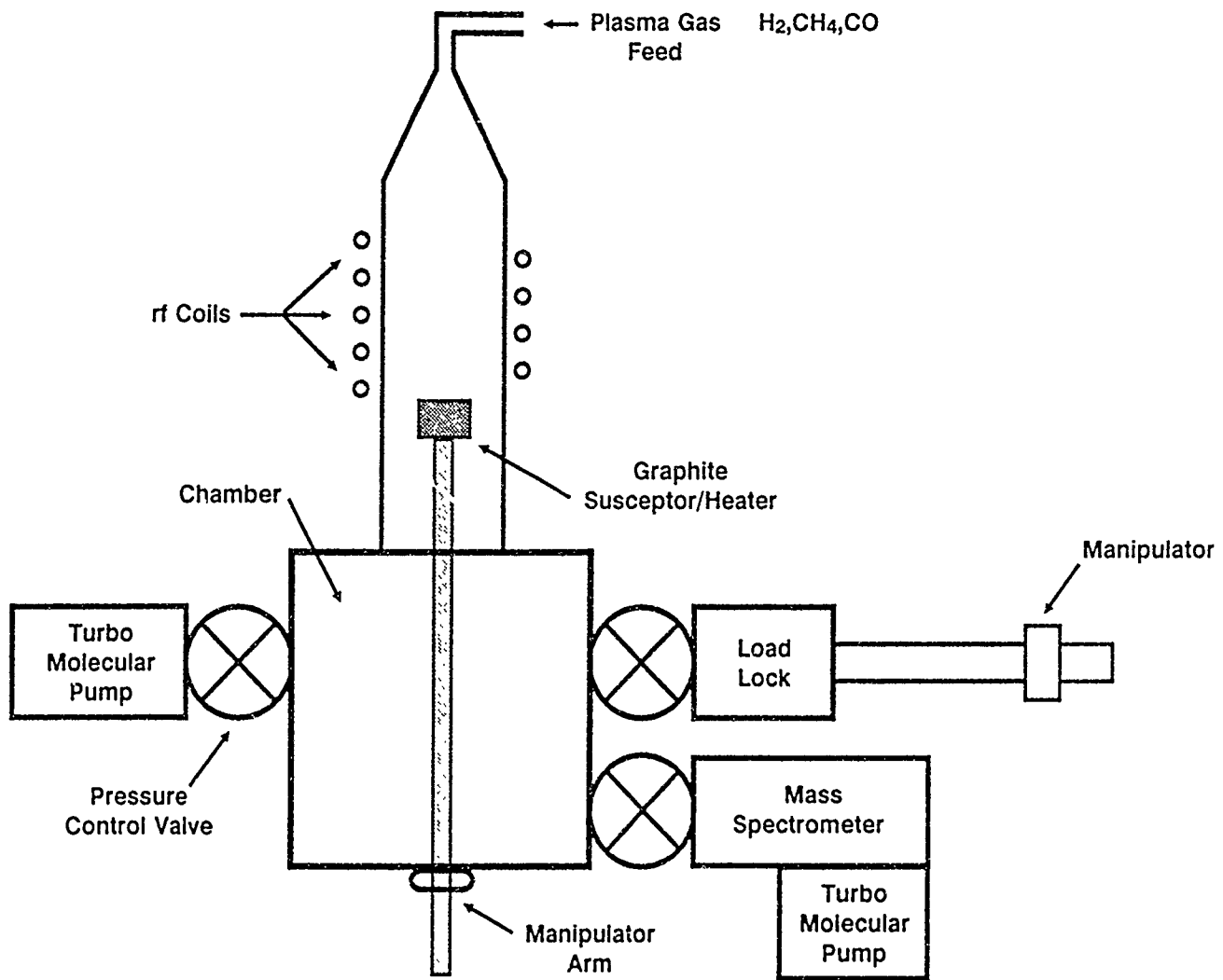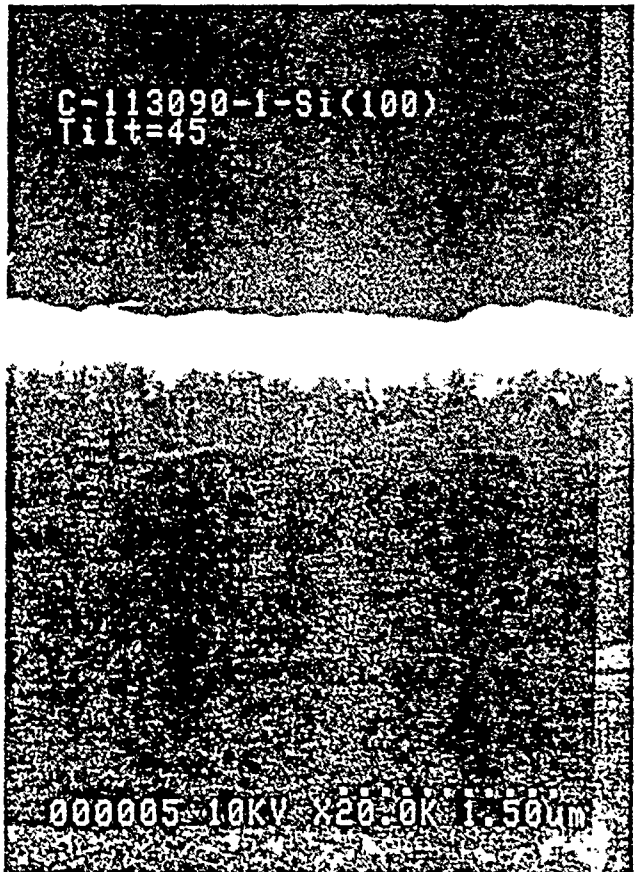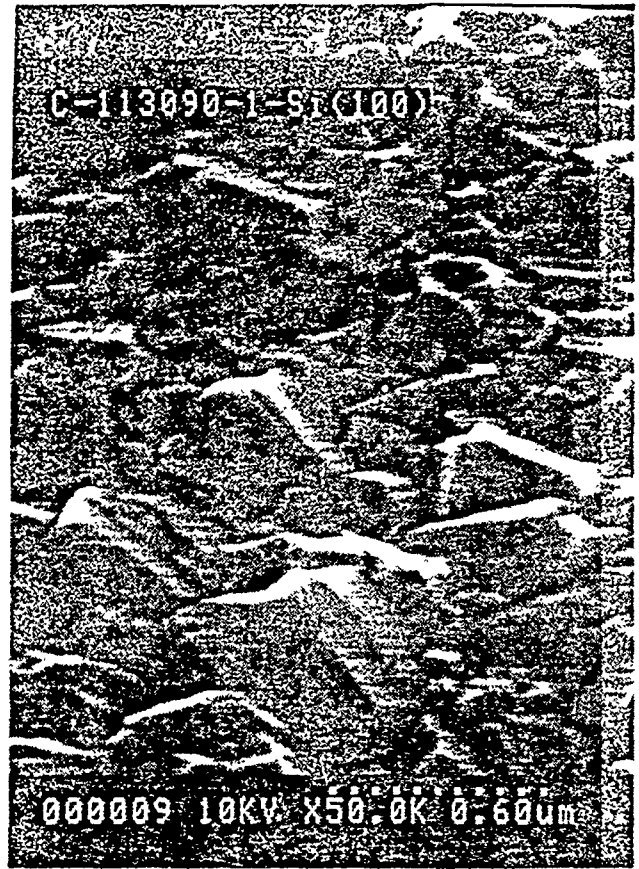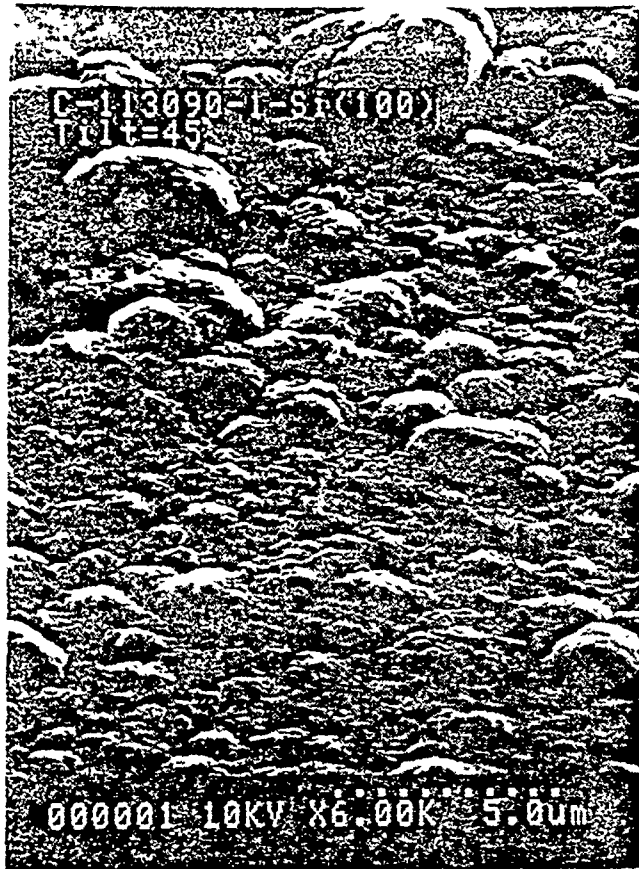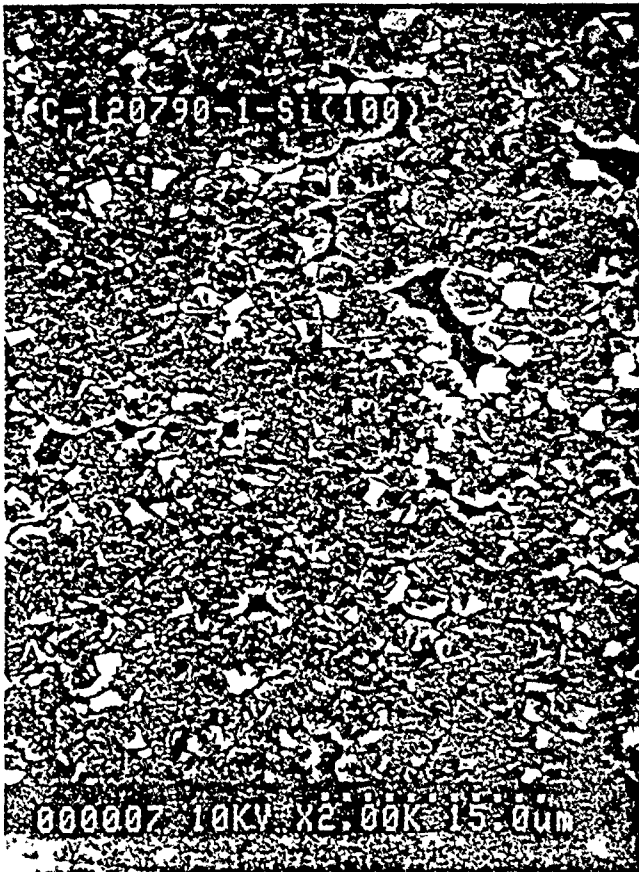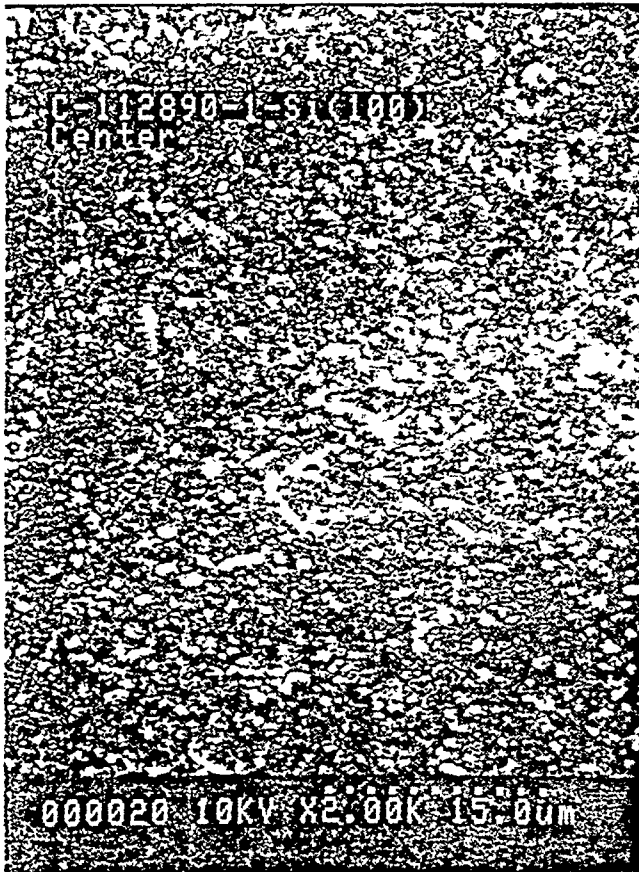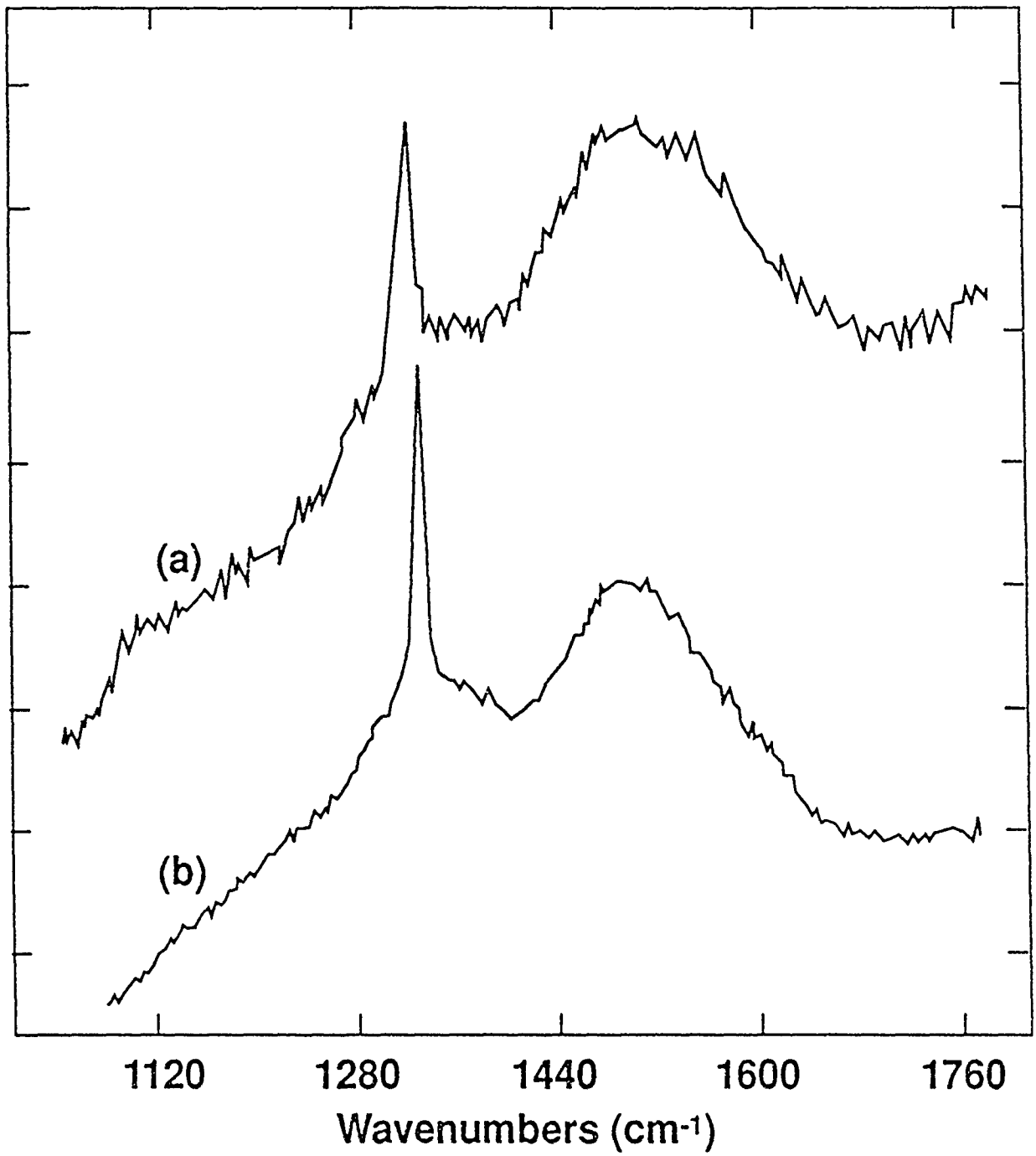
Plasma Gas Feed — H₂,CH₄,CO

rf Coils

Graphite Susceptor/Heater

Chamber

Manipulator

Turbo Molecular Pump

Load Lock

Pressure Control Valve

Mass Spectrometer

Turbo Molecular Pump

Manipulator Arm

FIGURE 1.

FIGURE 2.

53

FIGURE 3.

(a)

(b)

FIGURE 4.

55

6.0   LOCAL ENHANCEMENT OF DIAMOND NUCLEATION

Enhancement of diamond nucleation by graphite fibers local to substrate surfaces in H_2 - CH_4 rf discharges. R.A. Rudder, G.C. Hudson, R.C. Hendry, R.E. Thomas, J.B. Posthill, and R.J. Markunas. Research Triangle Institute, Research Triangle Park, NC 27709-2194.

It has been observed that the presence of graphite fibers tangential to a substrate surface greatly enhances the nucleation of diamond crystals immediately underneath the fiber. Silicon, nickel, fused silica, and crystalline quartz substrates following exposures to 2% CH_4 in H_2 rf-discharges show diamond growth along lines and in small clusters. The substrates were inserted into the reactor without any diamond polishing or surface treatments. The deposition patterns on the substrates mimic the placement of graphite fibers on the substrates prior to diamond growth. The fibers used in this work were taken from a yarn of material composed of 3-5 μm diameter carbon-graphite fibers. The carbon fibers are not composed of highly oriented graphite. Many of the fibers following exposure to the H_2 - CH_4 discharge show dense clusters of fine grain polycrystalline dir ond. Some fibers are completely enclosed with this fine g.ain diamond. Some fibers are void of diamond deposition. These fibers do not appear to have been etched by the atomic hydrogen ambient present from the rf discharge. Diamond deposition on the substrates underneath the fibers show clear facetting with lines of individual crystals Each line consists of colinear,

contiguous crystallites. Other areas show dense diamond nucleation and nearly a continuous diamond film with clearly-defined facets. These areas are 100-500 μm^2 in size. It is suspected that a cluster of fibers existed over that area during deposition. Cleaved sectional analysis of the colinear crystallites does not show the presence of an inner graphite core. The crystals on Si wafers strongly adhere to the substrate. The cleavage process frequently left pits on the Si surface where presumably a diamond crystallite had been removed by the fracture. Hence. the linear diamond growth on the substrates cannot be attributed to diamond deposition on a fiber resting on the surface of the substrate.

Local Enhancement of Diamond Nucleation near Fibers

On As-Received Si Wafers   On Fiber

7.0 CONCLUSIONS

The past year at Research Triangle Institute has been an extremely exciting one. We have seen the advancement of existing technologies such as the low pressure rf-plasma assisted CVD technology and the development of new techniques for diamond deposition with an emphasis on increasing diamond heteronucleation.

- Epitaxial lateral overgrowth was demonstrated;
- Diamond Schottky devices were fabricated with Li doping;
- Boron doped IGFETs were fabricated and tested;
- Gas analysis identified C_2H_2 by-product;
- Mo interlayers were deposited on Ni for heteronucleation studies;
- Hydrogen-halogen exchange reactions were demonstrated;
- A CF_4/H_2 system produced direct nucleation on Si(100);
- Nucleation enhancement local to graphite fibers was demonstrated.

This work would not have been possible without many local and national collaborations that are continuing and developing. These collaborations have included:

Contributed Work
- Physics Department, North Carolina State University
  R.J. Nemanich and T.P. Humphreys
- Naval Research Laboratory
  Jim Butler and Pehr Pehrsson
- Materials Science Department, North Carolina State University
  Yong-Hee Lee and Klaus Bachmann
- Kobe Steel Research Laboratories, Research Triangle Park, North Carolina
  V. Venkatesan and K. Das
- Physics Department, University of North Carolina
  Nalin Parikh and Max Swanson
- National Institute of Standards and Technology
  David Black
- Fiber Materials Incorporated, Biddeford, Maine
  Daniel Nelson

Discussions and Exchange of Information

- Chemistry Department, University of Pittsburg
  John Yates
- Chemical Engineering Department, Case Western Reserve University
  John Angus
- Aerodyne Research Incorporated
  Andrew Freedman